

Reinterpreting Survival Analysis in the Universal Approximator Age

Sören Dittmer

SD870@CAM.AC.UK

*Cambridge Image Analysis Group, University of Cambridge, UK
Center for Industrial Mathematics, University of Bremen, Germany*

Michael Roberts

MR808@CAM.AC.UK

Cambridge Image Analysis Group, University of Cambridge, UK

Jacobus Preller

JACOBUS.PRELLER1@NHS.NET

Department of Medicine, University of Cambridge, UK

AIX COVNET

Cambridge Image Analysis Group, University of Cambridge, UK

James H.F. Rudd

JHFR2@CAM.AC.UK

Department of Medicine, University of Cambridge, UK

John A.D. Aston

JADA2@CAM.AC.UK

Statistical Laboratory, University of Cambridge, UK

Carola-Bibiane Schönlieb

CBS31@CAM.AC.UK

Cambridge Image Analysis Group, University of Cambridge, UK

Abstract

Survival analysis is an integral part of the statistical toolbox. However, while most domains of classical statistics have embraced deep learning, survival analysis only recently gained some minor attention from the deep learning community. This recent development is likely in part motivated by the COVID-19 pandemic. We aim to provide the tools needed to fully harness the potential of survival analysis in deep learning. On the one hand, we discuss how survival analysis connects to classification and regression. On the other hand, we provide technical tools. We provide a new loss function, evaluation metrics, and the first universal approximating network that provably produces survival curves without numeric integration. We show that the loss function and model outperform other approaches using a large numerical study.

Keywords: Deep learning, Survival analysis, Classification, Regression

Code available at https://github.com/sdittmer/survival_analysis_sumo_plus_plus

1 Introduction

Survival analysis (SA) is a well-established branch of statistics Cox and Oakes (2018); Kalbfleisch and Prentice (2011); Kleinbaum et al. (2012); Yang et al. (2011); Han et al. (2016). Nevertheless, it has only recently been encountered in the world of machine learning and, even more recently, deep learning (DL) Lee et al. (2015); Kong et al. (2018); Lee et al. (2018); Giunchiglia et al. (2018); Ching et al. (2018); Yang et al. (2018); see Wang et al. (2019); Sonabend (2021) for an overview on classical machine learning for SA. As the DL community has only just started focusing on SA, many fundamental questions remain unsettled.

This paper aims to provide the tools to make SA as valuable for the DL community as possible through four main contributions. 1. We examine how SA can bridge the well-studied domains of classification and regression. 2. We propose a novel loss function for SA in the continuous-time setting. 3. We present the first DL model that provably produces survival curves in continuous time without the need for numeric integration methods and is also a universal approximator. 4. We propose a modified integrated Brier score incorporating classifier metrics for a more nuanced evaluation of highly expressive survival models.

We hope our contributions will enable a more flexible and widespread application of SA in DL. As one can apply SA to predict death, but also the occurrence of any event, we see great potential for deeper integration of the two subjects. For example, there is a significant interest in applying SA to a variety of data modalities, e.g., omics data Zhang et al. (2022) and imaging data Shahin et al. (2022). Particularly since 2020, with its utilization during the COVID-19 pandemic Wiegand et al. (2022); Crooks et al. (2020); Schwab et al. (2021), there has been increased interest in the adoption of deep learning for SA.

We will now describe the structure of the paper and its relation to previous work on the subject.

In Section 2, we examine the relationship between SA, classification, and regression. This connection has been partially examined in prior works such as Zhong and Tibshirani (2019), but not yet thoroughly. Other classification-inspired works have adapted binary cross-entropy losses for SA Lee et al. (2018); Ren et al. (2019). Our approach differs by formulating a loss function for continuous time settings, leveraging a probabilistic perspective.

In Section 3, we first extend the monotonically increasing MONDE networks Chilinski and Silva (2020) by improving their ability to model complex survival curves. Secondly, we modify the SuMo networks Rindt et al. (2022) to not only enable universal approximation but to guarantee that any output is a survival curve. This modification also brings the SuMo network’s formulation closer to one of classical survival models.

In Section 4, we implement a neural network version of the well-known Cox model and its time-dependent variant using methods from Section 3. This synthesis enables flexible training setups for Cox models and, especially for the time-dependent model, combines the excellent approximation properties of neural nets with the interpretability of Cox models. The papers Katzman et al. (2018); Shahin et al. (2022); Kvamme et al. (2019) are closest to this part of our work. But, in contrast, these papers replace the Cox model’s linear regression with a neural network, not their baseline function.

In Section 5, we provide a large-scale comparison of different survival models trained with different loss functions. We use seven datasets, one includes image data, and two are originally regression datasets, demonstrating the applicability of survival models to regression tasks. We choose these datasets for their diversity and to analyze our methodology on real-life datasets. Here we also introduce the modified integrated Brier scores Graf et al. (1999). Along with the established concordance index, they open up a rich pool of well-known quality measures, enabling a nuanced exploration of different aspects of a given model.

2 Reinterpreting survival analysis

We now discuss how SA can be a portal between classification and regression.

To set the stage, we introduce some key notation. We describe a potentially right-censored survival data sample via

$$(x, e, T) \in \mathbb{R}^n \times \{0, 1\} \times \mathbb{R}_{>0}, \quad (1)$$

where $x \in \mathbb{R}^n$ denotes input features, $e \in \{0, 1\}$ indicates if the event was observed (1) or not (0), and T is the time of the event or the time of right-censoring. We set $T > 0$ as one usually assumes that no events occur for $T \leq 0$.

The goal of SA is to use a set of such samples to create a model that uses the features x to predict the probability of a singular event, such as death, occurring after any given time $t \geq 0$. One assumes that the event has not occurred at $t = 0$ and is irreversible. Hence, one aims to produce a non-negative, monotonically decreasing curve being 1 at time $t = 0$. Throughout this paper, we will use the terms “alive” and “dead” to refer to the state before and after the singular event.

2.1 Survival analysis is classification (with infinitely many classifiers)

We will pose SA in terms of classification. We begin by recalling the general definition of a survival curve:

$$S(t|x) : \mathbb{R}_{\geq 0} \times \mathbb{R}^n \mapsto \mathbb{P}(\text{alive}@t|x) \in [0, 1] \quad (2)$$

That is, $S(t|x)$ gives us the probability that the event has not occurred before or at time t , given the features x .

An alternative way of reading this definition is that S is equivalent to a set of probabilistic binary classifiers

$$\{S(t|\cdot) = C_t : \mathbb{R}^n \rightarrow [0, 1] : t \in \mathbb{R}_{\geq 0}\}, \quad (3)$$

each $C_t(x)$ being the probability of surviving the interval $[0, t]$ given the features x . Phrased differently, *a survival model is simply an infinite collection of probabilistic classifiers indexed by time.*

Using the classifier perspective, we will derive a new loss function for survival curves. Considering the ideal scenario of having unlimited clean data and a highly capable probabilistic classifier, we can train one classifier for each point in time. This transforms the problem into a prediction of Bernoulli variables, and thus each classifier can be trained using the binary cross entropy (BCE) loss.

As a reminder, the standard BCE loss for a classifier $C : \mathbb{R}^n \rightarrow [0, 1]$ and a sample $(x, y) \in \mathbb{R}^n \times \{0, 1\}$ is defined as

$$-y \log C(x) - (1 - y) \log (1 - C(x)). \quad (4)$$

Returning to the SA setting, if we have a censored sample, $(x, 0, T)$, we can use it to train all classifiers before the censoring,

$$\{C_t : \mathbb{R}^n \rightarrow [0, 1] : t \in [0, T)\}, \quad (5)$$

via the BCE part

$$-\log C_t(x), \quad (6)$$

i.e., for censored samples, we want to find classifiers that predict 0 (“alive”) for times before the censoring.

Otherwise, if we have an uncensored sample, $(x, 1, T)$, we can use the loss in (6) for the early (“premortem”) classifiers given by (5) and train the later (“postmortem”) classifiers given by

$$\{C_t : \mathbb{R}^n \rightarrow [0, 1] : t \geq T\} \quad (7)$$

via the BCE part

$$-\log(1 - C_t(x)). \quad (8)$$

We can formulate a joint loss for all classifiers by choosing two arbitrary random variables, $\mathcal{T}_-(e, T)$ and $\mathcal{T}_+(e, T)$, with an everywhere-supported density over $[0, T]$ and $[T, \infty)$ respectively. We define this loss by joining (6) and (8) to

$$L_{\text{BCE}} = -[\mathbb{E}_{t_- \sim \mathcal{T}_-} \log S(t_- | x) + e \cdot \mathbb{E}_{t_+ \sim \mathcal{T}_+} \log (1 - S(t_+ | x))]. \quad (9)$$

The loss trains a separate classifier $S(t|\cdot) = C_t(x)$ for every point in time $t \in [0, \infty)$, as both \mathcal{T}_\pm are supported everywhere. We can consider the loss as a weighted integral over the BCE loss. As a result, it inherits many desirable properties of the BCE loss, such as being a strictly proper scoring rule Du (2021).

In practice, assuming an infinite amount of clean data is unrealistic. However, we have two advantages when dealing with commonly found un- and right-censored data. Firstly, earlier classifiers can use most data points (as little censoring has occurred yet). Secondly, as survival curves decrease over time, later classifiers’ predictions are upper bounded by earlier classifiers. To take advantage of this, we need to ensure the monotonicity of our predicted survival curves, which we will discuss in Section 3.

If the monotonicity holds, we also do not require that the density of \mathcal{T}_\pm is supported everywhere, as later classifiers provide lower bounds for earlier ones. In practice, we therefore do the following: We sample times from a Gaussian centered at T for uncensored samples and only from the left side of that Gaussian for censored samples. We ensure no negative time samples via projection with ReLU. The idea is that while one trains for all t , the Gaussian focuses the training effort on values around T ; here, the variance σ^2 is a hyperparameter that controls the focus. Other choices are plausible, but we leave this to future

work. Formally, we can represent this as

$$\mathcal{T}_-(e, T) = \begin{cases} \delta(T), & \text{if } e = 0, \\ \text{ReLU}_\# \mathcal{HN}_-(T, \sigma^2), & \text{otherwise,} \end{cases} \quad (10)$$

and

$$\mathcal{T}_+(e, T) = \mathcal{HN}_+(T, \sigma^2), \quad (11)$$

where δ denotes the delta-distribution, \mathcal{HN}_\pm the left- and right-sided half-normal distribution, and $\text{ReLU}_\#$ the pushforward operator of the projection into the non-negative real numbers.

During training, we approximate the expectations in (9) by sampling only one t . If $e = 0$ we sample $t \sim \mathcal{T}_-$, if $e = 1$, we sample with a 50% probability from \mathcal{T}_- otherwise from \mathcal{T}_+ .

As a comparison, we use the SuMo loss Rindt et al. (2022)

$$L_{\text{SuMo}} = -[e \log f(t|x) + (1 - e) \log S(t|x)], \quad (12)$$

where

$$f(t|x) = -\partial_t S(t|x). \quad (13)$$

Both losses can be seen as log-likelihoods and are similar in their $e = 1$ part but differ in their $e = 0$ part. This is because SuMo’s likelihood is conditioned on the event variable e , while the BCE’s is not.

2.2 Survival analysis is regression (with uncertainty estimation)

We will now discuss how we can use a survival model to predict the full posterior of $\mathbb{R}^n \rightarrow \mathbb{R}_{\geq 0}$ regression problems. The idea is similar to the motivation of the paper Chilinski and Silva (2020). Using (2), we can express the lifetime distribution function (probability of the event has not occurred yet) as

$$F(t|x) = \mathbb{P}(\text{dead}@t|x) = 1 - S(t|x). \quad (14)$$

Consequently, we can interpret $f(t|x)$ as an event density.

We now want to make a simple but powerful observation. We can treat any dataset with non-negative scalar labels as an uncensored survival dataset. Consequently, the event density f of a survival model that fits the dataset well (see Section 3) is the full posterior of the original regression problem.

Note that this setup also allows one to train regression models on samples for which one only knows a lower bound on the label.

2.3 If in doubt: survival analysis

SA can be viewed from both a classification and regression perspective. Understanding this duality is beneficial when selecting a model or interpreting results. Any one-dimensional regression problem or binary classification involving a threshold can benefit from this perspective by rephrasing the question one asks. For example, the clocks dataset Verma (2019) provides images of analog clocks with the displayed times as labels; see Figure 1 for two

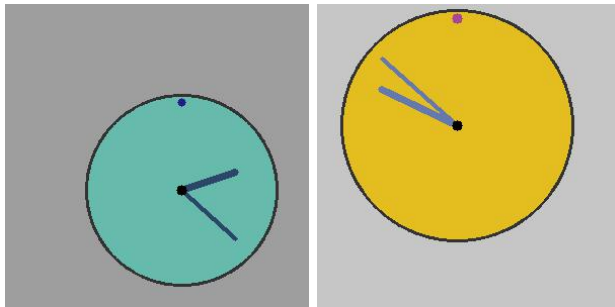


Figure 1: Two samples from the Clocks dataset Verma (2019).

samples. We can interpret the dataset as asking: “what time does the clock show?”; this is a regression problem. Alternatively, we could ask for any point in time: “is it earlier than the time the clock shows?”; this subtle shift in question turns the regression into a classification problem. Training a survival model instead of a regression or classification model can answer both questions and many others.

The ability of survival models to answer various questions at inference time is a strong advantage (particularly those not considered during training). Another benefit of framing a problem as a survival problem, where possible, is that the training process receives more information per label. While classification uses binary information about which side of a threshold the value is on, SA uses the value itself.

3 A universal and exclusive survival curve approximator

We will now introduce MONDE+, a version of MONDE Chilinski and Silva (2020) more capable of modeling complex survival curves, and SuMo++, an improved version of SuMo Rindt et al. (2022) that now guarantees $S(0|x) = 1$ and uses MONDE+. This makes the model not only a universal but also an exclusive approximator of survival curves, by which we mean that the model is capable of approximating any survival curve and incapable of producing anything but a survival curve. For a review of MONDE and SuMo, see appendix, Section A. We also refer to Saul (2016) for universal approximators derived via Gaussian processes and Danks and Yau (2022) for ones derived via numeric integration of neural networks.

We start by introducing the notation for the cumulative hazard function, $\Lambda(t|x)$, defined via

$$S(t|x) = \exp[-\Lambda(t|x)]. \quad (15)$$

One can interpret Λ as the total accumulated risk. Since Λ determines the model, building a good survival model is equivalent to building a good model for Λ . The model should be flexible enough to approximate any cumulative hazard. To guarantee survival curves, we have to ensure that Λ is monotonically increasing and $\Lambda(0|\cdot) = 0$.

3.1 MONDE+

As the main building block for such Λ we now define the MONDE+ network

$$M_+ : \mathbb{R} \times \mathbb{R}^n \ni (t, x) \mapsto M_+(t, x) \in \mathbb{R}. \quad (16)$$

It is monotonically increasing in its first argument and we define it via layers

$$z_{k+1}(t, z_k, z_0) = H_k z_k + \sigma_k(\tilde{z}_k(t, z_k) + B_k z_k + L_k z_0) \quad (17)$$

with

$$\tilde{z}_k(t, z_k) = A_k (\phi_k(a_k t + b_k) \circ \psi_k(G_k z_k)) \quad (18)$$

where a_k and b_k are vectors, all capitalized letters represent affine maps, and \circ denotes the Hadamard product. σ_k, ϕ_k , and ψ_k are monotonically increasing functions with non-negative ϕ_k and ψ_k . In practice, we use $\phi_k = \psi_k = \text{softplus}$ and $\sigma_k = \text{tanh}$, in the last layer we set $\sigma_K = \text{id}$. Similar to MONDE, we constrain the weight matrices of A_k, B_k, G_k , and H_k and the vector a_k to be pointwise non-negative. Refer to Section B of the appendix for details on the initialization.

We recall that a MONDE network $M : \mathbb{R}^{n+1} \rightarrow \mathbb{R}$ consists of layers

$$z_{k+1}(z_k) = \sigma_k(B_k z_k), \quad (19)$$

i.e., they cannot differentiate inputs t, x , have no residual connections He et al. (2016), and are a strict subset of the MONDE+ layers.

Unlike MONDE, MONDE+ is monotone in t but has no unnecessary monotonicity constraint in x , see the following lemma.

Lemma 1 *Let $M_+ : \mathbb{R} \times \mathbb{R}^n \rightarrow \mathbb{R}$ be a MONDE+ network, i.e., a concatenation of layers defined by (17). Then the output of each layer of M_+ is pointwise monotonically increasing in t .*

For the proof, see Section C of the appendix. Each MONDE+ layer contains a MONDE layer as a subset of its operations. As the universal approximation properties of the MONDE network are already established Lang (2005), this also makes MONDE+ a universal approximator. As we will show in Section 5, the MONDE+ component within SuMo++ can successfully model the survival curves for a broad range of applications.

3.2 SuMo++

As previously stated, the SuMo++ network aims to improve SuMo’s ability to produce accurate survival curves while maintaining its theoretical guarantees of universal approximation.

We define the SuMo++ network as

$$\mathcal{S}_{++}(t, x) = \exp(-[M_+(t, q) - M_+(0, q)]), \quad (20)$$

i.e., we set the cumulative hazard function to

$$\Lambda(t|q) = M_+(t, q) - M_+(0, q) \quad (21)$$

with $q = Q(x) \in \mathbb{R}^k$ being some feature extracting network. The exponent in SuMo++ is monotonically decreasing in t and 0 for $t = 0$. Therefore, SuMo++ is not only monotonically decreasing with values in $[0, 1]$, but also guarantees $\mathcal{S}_{++}(0, x) = 1$.

In contrast, the SuMo network is defined via a MONDE network as

$$\mathcal{S}(t, x) = 1 - \text{sigmoid}(M([t, Q(x)])), \quad (22)$$

it can, at best, achieve $\mathcal{S}(0, x) = 1$ up to some error $\epsilon > 0$ since $\mathcal{S}(t, x) < 1$.

Note that alternatively, one could define SuMo++ via $\mathcal{S}_{++}(t, x) = \frac{1}{1+[M_+(t,q)-M_+(0,q)]}$. However, we did not see any difference in performance, but the former formulation leaves the model and its interpretability closer to classical formulation in (15).

We formulated SuMo++ in terms of MONDE+, but we could also do so via MONDE by splitting its input into $z = (t, x)$. For simplicity, we will refer to the SuMo++ approach using MONDE as SuMo+.

Now, as we have established a universal and exclusive approximator of survival curves, we will discuss how SuMo++ is also backward compatible, i.e., how we can use it and MONDE+ to parameterize and treat Cox models as neural networks.

4 Bringing (time-dependent) Cox models into the deep learning age

The Cox model, introduced in 1972 Cox (1972), is arguably the most popular survival model. It uses a baseline cumulative hazard function $\Lambda_0 : \mathbb{R}_{\geq 0} \ni t \mapsto \Lambda_0(t) \in \mathbb{R}_{\geq 0}$, that depends only on time, and a linear regression to modulate the hazard up and down based on the input features x . Formally we write

$$\mathcal{S}_{\text{Cox}}(t, x) = \exp(-\alpha(x)\Lambda_0(t)), \quad (23)$$

where

$$\alpha(x) = \exp(\langle a, x \rangle) \quad (24)$$

with the coefficient $a \in \mathbb{R}^n$. This approach seems to strike an outstanding balance between expressiveness and interpretability.

We now describe what we believe is the first implementation of the Cox (and later time-dependent Cox) model that directly parameterizes Λ_0 via a neural network. Note, for the Cox model, Danks and Yau (2022) implements Λ_0 indirectly via a neural network but requires the numeric integration of it.

4.1 A neural network parameterized Cox model

We will now introduce a neural network-based implementation of the classical Cox model. While we will use MONDE+ and SuMo++, the following formulations also hold for MONDE and SuMo+ but not SuMo.

The function Λ_0 is monotonically increasing, with 0 as a fixed point, and can be parameterized in different ways, e.g., by splines Efron (1988); Royston and Parmar (2002) or in a non-parametric fashion Crowley and Breslow (1984). We will do so using neural networks.

Using the results in Section 3, we can parameterize a Cox model by setting

$$\Lambda_0(t) = M_+(t, 0) - M_+(0, 0) \quad (25)$$

and obtain

$$\mathcal{S}_{\text{Cox}}(t, x) = \exp(-\alpha(x)\Lambda_0(t)) = \mathcal{S}_{++}(t, 0)^{\alpha(x)}. \quad (26)$$

We want to emphasize that in contrast to the DeepSurv model (also known as DeepHit) independently introduced by Katzman et al. (2018), Lee et al. (2018) and Shahin et al. (2022), we propose a parameterization for Λ_0 . This makes our approach not a modification, but an implementation, of the Cox model and, therefore, equally interpretable. Still, we enable training and evaluation within DL frameworks using automatic differentiation Paszke et al. (2017). This enables not only easy training of Cox models using different loss functions, but also straightforward computation of the event density, $f = -\partial_t S$, and hazard function $\lambda(t|x) = \partial_t \Lambda(t|x)$.

4.2 A neural network parameterized time-dependent Cox model

We will now show how we can parameterize Cox models with time-dependent coefficients Fisher et al. (1999) using neural networks. These models are of the form

$$\mathcal{S}_{\text{COX}}(t, x) = \exp(-\alpha(t, x)\Lambda_0(t)), \quad (27)$$

where one usually sets $\alpha(t, x) = \exp[\langle \omega(t), x \rangle]$ with $\omega : \mathbb{R}_{\geq 0} \rightarrow \mathbb{R}^n$.

Again, as in Section 4.1, we can parameterize $\Lambda_0(t)$ via (25). For α , we propose the parametrization

$$\alpha(t, x) = \exp(\langle \omega(t, x), |x - o| \rangle) \quad (28)$$

where $|\cdot|$ is the entrywise absolute value and $o \in \mathbb{R}^n$ a learnable offset parameter. We use two MONDE+ networks M_{\pm}^{\pm} to define $\omega : \mathbb{R}_{\geq 0} \times \mathbb{R}^n \rightarrow \mathbb{R}^n$ entrywise as

$$\omega_i(t, x) = \begin{cases} \beta_i^-(t), & \text{if } x_i < o_i, \\ \beta_i^+(t), & \text{otherwise,} \end{cases} \quad (29)$$

where we set $\beta^{\pm} : \mathbb{R}_{\geq 0} \rightarrow \mathbb{R}^n$ to

$$\beta^-(t) = M_{\pm}^-(t, 0) - M_{\pm}^-(0, 0) + M_{\pm}^+(0, 0) \quad (30)$$

and

$$\beta^+(t) = M_{\pm}^+(t, 0). \quad (31)$$

Unlike in Section 4.1, this is not just a reparametrization but a slight modification guaranteeing $\mathcal{S}_{\text{COX}}(t, x)$ to decrease monotonically in t , see Lemma 2. Still, the coefficients ω are highly interpretable, as they separate the effects of t from x . Essentially, ω_i provides a time-dependent weight for x_i that is independent of x except for the threshold o_i , which marks the “least dangerous” value x_i can take.

Lemma 2 *For the model $\mathcal{S}_{\text{COX}}(t, x)$, defined by (27) and (28), it holds $\forall x \in \mathbb{R}^n$ that:*

1. $\mathcal{S}_{\text{COX}}(t, x) \in [0, 1]$ for all $t \in \mathbb{R}_{\geq 0}$.
2. We have a maximum $\mathcal{S}_{\text{COX}}(0, x) = 1$.
3. $\mathcal{S}_{\text{COX}}(t, x)$ is monotonically decreasing in t .

Further, if the M_{\pm}^{\pm} are continuous in t , we have:

1. The ω_i are continuous in t .
2. For any x , the $\omega_i(\cdot, x)$ have their minima at $\omega_i(0, x) = \beta_i^+(0)$.
3. α is continuous in (t, x) .

See Section D of the appendix for the proof.

5 Numerical experiments

We will now present the results of our numerical experiments. We will first compare the performance of MONDE and MONDE+ and then perform an extensive comparison of different survival models using several survival and regression datasets.

5.1 MONDE vs. MONDE+: A toy example

We now compare the performance of the SuMo, SuMo+, and SuMo++ networks – i.e., MONDE without and with the initial condition enforced and MONDE+ with the initial condition enforced.

To showcase the limitations of the SuMo and SuMo+ models in recreating survival curves, we designed an experiment using six samples, each containing 32 features, each in the range $[-1, 1]$. We assigned survival probabilities for each sample at 2-7 points over the time interval $[0, 1]$ in a way that tests the models’ ability to capture complex distributions, such as sharp declines followed by plateaus and vice versa.

We trained each network for 512 Adam Kingma and Ba (2014) iterations with a step size of 10^{-3} using the standard binary cross-entropy loss. Figure 2 compares the three models over the six samples. To show the variability of the outcome, we also provide histograms of multiple runs of these experiments in Figure 3. The histograms show that it can be difficult for the SuMo+ model to fit the six curves, while the SuMo and SuMo++ can produce better fits.

During these and all following experiments, we used MONDE+ with five hidden layers of width 32. We also use MONDE with the same structure, but after the input layer, we change the width to 98 to give both networks approximately 32,000 trainable parameters.

5.2 Classifier metrics

We will now discuss how we will evaluate the following experiments. As discussed in Rindt et al. (2022), the classical scoring rules for survival models do not adequately reflect the performance of survival models. Classical scoring rules for survival models, such as time- or hazard-based concordance scores for traditionally trained Cox models, are only effective in their intended context. However, they may not accurately reflect performance in a general setting defined by (2). For example, a model that incorrectly predicts all patients dying within milliseconds of a clinical trial may still have a perfect concordance score, as the score only considers the correct order of events and not their absolute time. This does not make time concordance useless for these models but insufficient. Ideally, one would have multiple scoring rules to choose from to judge the different aspects of a model that are relevant to a given situation.

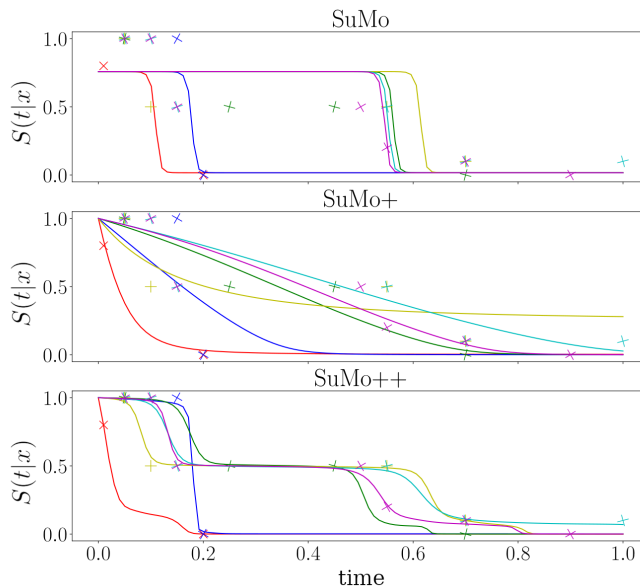


Figure 2: Points and their corresponding learned curves are color-matched. To distinguish overlapping points, we use crosses with varying rotations. Each of the three plots is the result of one training. The plots correspond to the losses of 2.5, 2.6, and 1.7 (top to bottom). The top plot shows that the SuMo network can produce curves that do not fulfill survival curve’s initial condition $S(0|x) = 1$.

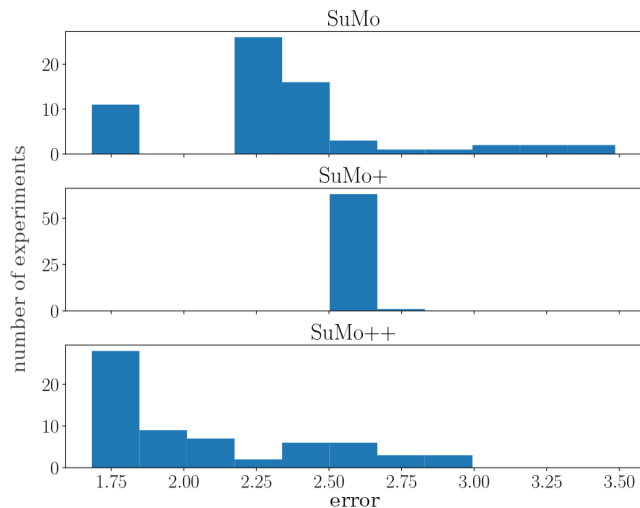


Figure 3: BCE loss histograms of the different networks. Each contains 64 training runs with 512 training steps each. To see the results after convergence (2048 steps), see Figure 4 in the appendix. Figure 4 shows that both SuMo+ and SuMo++ benefit from further training steps – SuMo+ almost improves to the level of SuMo++ – while SuMo shows no significant improvement.

Name	#Samples	#Features	Test set
GBSG2	686	8	25%
Recur	1,296	4	25%
NKI	272	9	25%
Lymph	686	8	25%
COVID-19	1,489	16	25%
Clocks	10,000	6,912	2.5%
California	20,640	8	2.5%

Table 1: An overview of the datasets as we used them. Up to rounding errors, we split the data such that the validation and test have the same size, i.e., if the test set contains 25% of the sample, the validation contains 25%, and the training contains 50% of the samples. For the references see, GBSG2 Sauerbrei and Royston (1999), Recur Lemeshow et al. (2011), NKI Nicolau et al. (2011), Lymph Schmoor et al. (2000), Clocks Verma (2019), and California Pace and Barry (1997).

We propose to use the general integrated Brier score (IBS). However, instead of using the mean squared as the integrated scoring rule, we propose to use general classifier scoring rules, e.g., accuracy. Interestingly this fits squarely into the original general definition of the IBS Graf et al. (1999), but we have not seen it applied this way.

As a survival model is an infinite number of probabilistic classifiers indexed by time, we can evaluate the survival model’s quality from different aspects; simply by choosing from the rich pool of classifier quality measures. E.g., one could use the F_2 -score if one considers a clinical setting where an overly optimistic prognosis may deny patients timely access to escalation.

Note that we will use threshold-free versions of all classifier scoring rules. For example, if $l \in \{0, 1\}^K$ is a binary vector of length $K \in \mathbb{N}$ containing labels and $p \in [0, 1]^K$ a vector containing corresponding probabilistic predictions, we define the true-positives to be their scalar product, i.e., $\sum_{k=1}^K p_k l_k$.

The IBS integrates its particular scoring rule over a given time interval. We will use the interval $[0, T_{max}]$ where we choose T_{max} for each dataset based on the 90th percentile of times provided by the dataset.

The mean squared error is arguably the most popular scoring rule in regression. Thus the standard IBS neatly connects to the regression point of view we laid out in Section 2.2, while the classifier scoring rules proposed by us connect to Section 2.1.

5.3 Datasets

We will now provide a brief qualitative overview of the datasets we use in Section 5.4. See Table 1 for a high-level overview. Each dataset consists of samples given by triples as in (1) i.e., (x, e, T) . We convert the Clocks and California regression datasets into this format by assigning T the label’s value and $e = 1$.

The COVID-19 dataset is a private dataset based on COVID-19 patient data from Addenbrooke’s Hospital, Cambridge, UK. The seven datasets showcase diverse survival

curve dynamics. For example, the dynamics of oncology treatment outcomes and that of critically ill patients differ greatly. The Clocks dataset, with deterministic outcomes, highlights sudden changes in survival curves.

As some of the datasets have relatively few samples, the random seed used to split the data into training, validation, and test sets can significantly impact the evaluation of a model. To mitigate this effect, we ran 1000 splits and selected the seed that minimizes the difference between the three Kaplan-Meier estimators for the training, validation, and test sets. Since Kaplan-Meier estimates the expected unconditioned survival curve for each set, this decreases the chance of having vastly different training, validation, and test sets.

We normalize all input features to have a 0 mean and standard deviation of 1. We normalize the times within the data by dividing through by T_{max} as defined in Section 5.2. For more details on the datasets, see Section E in the appendix.

5.4 Results and discussion

For the Clocks dataset, containing images, we apply the methods amenable to convolutions to extract the features for the model, namely CoxDeepNN, SuMo, SuMo+, and SuMo++, as well as Kaplan-Meier. For all other datasets, which contain tabular data, we were able to train all models discussed earlier. See Section F in the appendix for training details. We used the standard and classifier metric versions of the IBS discussed in Section 5.2 to evaluate the models. We use the classifier metrics accuracy, area under the precision-recall curve (AUPRC), area under the receiver operating characteristic curve (AUROC), balanced accuracy, the F_β -score for $\beta \in \{0.5, 1, 2\}$, precision, sensitivity, specificity, and the Youden’s index Youden (1950). In addition to the IBS, we also used the established concordance index based on the restricted mean survival time, restricted by the dataset’s T_{max} . See Table 8 and Table 17 in the appendix for the concordance index and the standard IBS. We report the mean of all scores in Table 2. Note that the CoxDeepNN model approach is well known from other papers Katzman et al. (2018); Kvamme et al. (2019); Shahin et al. (2022), commonly referred to as DeepHit or DeepSurv.

In Section H of the appendix, we present tables with each separate integrated quality score, along with the non-integrated versions of the balanced accuracy and the F_1 score for each dataset in Section I. We chose these two scores as they are highly correlated with the mean of the scores and complement each other.

Table 2 shows that SuMo, SuMo+, and SuMo++ outperform all other models. For example, plots of survival curves see Section J in the appendix. In particular, SuMo+ and SuMo++ slightly outperform SuMo in most cases while guaranteeing the output to be a survival curve. For the losses, the BCE loss tends to outperform the SuMo loss on survival datasets containing right-censoring; for more on the SuMo loss, see the appendix, Section F, and Rindt et al. (2022).

In contrast, the SuMo loss outperforms the BCE for the adapted regression datasets. We are not sure why that is, but the SuMo, unlike the BCE loss, is conditioned on whether the event was observed. This might decrease its performance if censoring is not independent of the time of the event. This would not be an issue for an entirely uncensored dataset.

Model Loss-function	COVID-19	NKI	BGS2	Recur	Lymph	Clocks	California
Kaplan-Meier	0.40	0.43	0.45	0.52	0.42	0.51	0.52
Weibull	0.67	0.52	0.51	0.75	0.47	\emptyset	0.68
Log-logistic	0.67	0.53	0.51	0.76	0.47	\emptyset	0.71
Log-normal	0.67	0.53	0.51	0.76	0.48	\emptyset	0.70
Cox-piecewise	0.67	0.52	0.51	0.75	0.47	\emptyset	0.67
Cox-spline	0.67	0.52	0.51	0.75	0.47	\emptyset	0.67
CoxNN SuMo	0.70	0.54	0.50	0.77	0.49	\emptyset	0.68
CoxNN BCE	0.72	0.54	0.51	0.73	0.48	\emptyset	0.64
C \otimes xNN SuMo	0.73	0.56	0.51	0.79	0.50	\emptyset	0.65
C \otimes xNN BCE	0.70	0.56	0.51	0.79	0.48	\emptyset	0.62
CoxDeepNN SuMo	0.73	0.53	0.55	0.79	0.50	0.69	0.69
CoxDeepNN BCE	0.72	0.58	0.49	0.78	0.49	0.83	0.65
SuMo SuMo	0.73	0.55	0.49	0.80	0.50	0.97	0.80
SuMo BCE	0.74	0.62	0.54	0.81	0.47	0.91	0.77
SuMo+ SuMo	0.72	0.50	0.50	0.79	0.49	0.97	0.81
SuMo+ BCE	0.76	0.59	0.54	0.79	0.48	0.91	0.78
SuMo++ SuMo	0.73	0.57	0.53	0.80	0.49	0.96	0.80
SuMo++ BCE	0.72	0.64	0.55	0.79	0.52	0.91	0.78

Table 2: The mean of all over time integrated scores and the concordance index for each model and the relevant test dataset. The higher, the better. We only list our BCE loss and the SuMo loss if applicable. The CoxDeepNN model is also known as DeepHit or DeepSurv. For the individual scores see the appendix, Tables 5– 17.

6 Conclusion

In this paper, we accomplished four main objectives: 1. We examined how SA can bridge the well-studied domains of classification and regression. 2. We proposed a novel loss function. 3. We present the first DL model that provably produces survival curves in continuous time and is also a universal approximator. 4. We suggested a more nuanced evaluation of survival models by modifying the integrated Brier score with classifier metrics.

We also retrofitted our new models to the well-established Cox model and its time-dependent version. Further we conducted a comprehensive comparison of recent and traditional methods. Our novel BCE loss outperforms the SuMo loss and the classical setup on classical survival tasks. In contrast, the SuMo loss outperforms on reinterpreted regression tasks where no censoring is present.

Our work presents the potential for more powerful survival models in fields such as clinical data, engineering, economics, and sociology. Therefore we hope our reinterpretation and stronger models – applicable to modalities like images – open up SA to a broader audience.

While new DL approaches offer promising results, the quality of uncertainty estimation remains an open area of research. For example, our BCE loss is influenced by σ and distributions \mathcal{T}_{\pm} in (10) and (11), which can affect the final model. However, this can also

be an opportunity to adapt the model’s predictions based on the specific application and evaluation criteria. Finally, we want to point out that any survival model produces biased predictions if the censoring assumption, usually non-informative censoring, is violated.

Acknowledgments and Disclosure of Funding

There is no direct funding for this study, but the authors are grateful for the following indirect funding: The EU/EFPIA Innovative Medicines Initiative project DRAGON (101005122) (M.R., S.D., AIX-COVNET, C.-B.S.), the Trinity Challenge (M.R., C.-B.S.), the EPSRC Cambridge Mathematics of Information in Healthcare Hub EP/T017961/1 (M.R., S.D., J.H.F.R., J.A.D.A, C.-B.S.), the Cantab Capital Institute for the Mathematics of Information (C.-B.S.), the European Research Council under the European Union’s Horizon 2020 research and innovation programme grant agreement no. 777826 (C.-B.S.), the Alan Turing Institute (C.-B.S.), Wellcome Trust (J.H.F.R.), Cancer Research UK Cambridge Centre (C9685/A25177) (C.-B.S.), British Heart Foundation (J.H.F.R.), the NIHR Cambridge Biomedical Research Centre (J.H.F.R.), HEFCE (J.H.F.R.). In addition, C.-B.S. acknowledges support from the Leverhulme Trust project on ‘Breaking the non-convexity barrier’, the Philip Leverhulme Prize, the EPSRC grants EP/S026045/1 and EP/T003553/1 and the Wellcome Innovator Award RG98755. Finally, the AIX-COVNET collaboration is also grateful to Intel for financial support.

We also want to acknowledge and thank the members of the AIX-COVNET collaboration: Michael Roberts¹, Sören Dittmer^{1,6}, Ian Selby⁷, Anna Breger^{1,8}, Matthew Thorpe⁹, Julian Gilbey¹, Jonathan R. Weir-McCall^{7,10}, Effrossyni Gkrania-Klotsas³, Anna Korhonen¹¹, Emily Jefferson¹², Georg Langs¹³, Guang Yang¹⁴, Helmut Prosch¹³, Jacobus Preller³, Jan Stanczuk¹, Jing Tang¹⁵, Judith Babar³, Lorena Escudero Sánchez⁷, Philip Teare¹⁶, Mishal Patel^{16,17}, Marcel Wassin¹⁸, Markus Holzer¹⁸, Nicholas Walton¹⁹, Pietro Lió²⁰, Tolou Shadbahr¹⁵, James H. F. Rudd⁴, John A.D. Aston⁵, Evis Sala⁷ and Carola-Bibiane Schönlieb¹.

¹ Department of Applied Mathematics and Theoretical Physics, University of Cambridge, Cambridge, UK ² A list of authors and their affiliations appears at the end of the paper ³ Addenbrooke’s Hospital, Cambridge University Hospitals NHS Trust, Cambridge, UK. ⁴ Department of Medicine, University of Cambridge, Cambridge, UK ⁵ Department of Pure Mathematics and Mathematical Statistics, University of Cambridge, Cambridge, UK ⁶ ZeTeM, University of Bremen, Bremen, Germany ⁷ Department of Radiology, University of Cambridge, Cambridge, UK ⁸ Faculty of Mathematics, University of Vienna, Austria. ⁹ Department of Mathematics, University of Manchester, Manchester, UK. ¹⁰ Royal Papworth Hospital, Cambridge, Royal Papworth Hospital NHS Foundation Trust, Cambridge, UK ¹¹ Language Technology Laboratory, University of Cambridge, Cambridge, UK. ¹² Population Health and Genomics, School of Medicine, University of Dundee, Dundee, UK. ¹³ Department of Biomedical Imaging and Image-guided Therapy, Computational Imaging Research Lab Medical University of Vienna, Vienna, Austria. ¹⁴ National Heart and Lung Institute, Imperial College London, London, UK. ¹⁵ Research Program in Systems Oncology, Faculty of Medicine, University of Helsinki, Helsinki, Finland. ¹⁶ Data Science & Artificial

Intelligence, AstraZeneca, Cambridge, UK. ¹⁷ Clinical Pharmacology & Safety Sciences, AstraZeneca, Cambridge, UK. ¹⁸ contextflow GmbH, Vienna, Austria. ¹⁹ Institute of Astronomy, University of Cambridge, Cambridge, UK. ²⁰ Department of Computer Science and Technology, University of Cambridge, Cambridge, UK.

References

- Takuya Akiba, Shotaro Sano, Toshihiko Yanase, Takeru Ohta, and Masanori Koyama. Optuna: A next-generation hyperparameter optimization framework. In *Proceedings of the 25th ACM SIGKDD international conference on knowledge discovery & data mining*, pages 2623–2631, 2019.
- Steve Bennett. Log-logistic regression models for survival data. *Journal of the Royal Statistical Society: Series C (Applied Statistics)*, 32(2):165–171, 1983.
- Pawel Chilinski and Ricardo Silva. Neural likelihoods via cumulative distribution functions. In *Conference on Uncertainty in Artificial Intelligence*, pages 420–429. PMLR, 2020.
- Travers Ching, Xun Zhu, and Lana X Garmire. Cox-nnet: an artificial neural network method for prognosis prediction of high-throughput omics data. *PLoS computational biology*, 14(4):e1006076, 2018.
- David R Cox. Regression models and life-tables. *Journal of the Royal Statistical Society: Series B (Methodological)*, 34(2):187–202, 1972.
- David Roxbee Cox and David Oakes. *Analysis of survival data*. Chapman and Hall/CRC, 2018.
- Colin J Crooks, Joe West, Andrew Fogarty, Joanne R Morling, Matthew J Grainge, Sherif Gonem, Mark Simmonds, Andrea Race, Irene Juurlink, Steve Briggs, et al. Predicting the need for escalation of care or death from repeated daily clinical observations and laboratory results in patients with SARS-CoV-2 during 2020: a retrospective population-based cohort study from the United Kingdom. *medRxiv*, 2020.
- John Crowley and Norman Breslow. Statistical analysis of survival data. *Annual review of public health*, 5(1):385–411, 1984.
- Dominic Danks and Christopher Yau. Derivative-Based Neural Modelling of Cumulative Distribution Functions for Survival Analysis. In *International Conference on Artificial Intelligence and Statistics*, pages 7240–7256. PMLR, 2022.
- Cameron Davidson-Pilon. lifelines, survival analysis in Python, September 2022. URL <https://doi.org/10.5281/zenodo.7111973>. If you use this software, please cite it using these metadata.
- Hailiang Du. Beyond Strictly Proper Scoring Rules: The Importance of Being Local. *Weather and Forecasting*, 36(2):457–468, 2021.
- Bradley Efron. Logistic regression, survival analysis, and the Kaplan-Meier curve. *Journal of the American statistical Association*, 83(402):414–425, 1988.

- Lloyd D Fisher, Danyu Y Lin, et al. Time-dependent covariates in the Cox proportional-hazards regression model. *Annual review of public health*, 20(1):145–157, 1999.
- John W Gamel and Ian W McLean. A stable, multivariate extension of the log-normal survival model. *Computers and Biomedical Research*, 27(2):148–155, 1994.
- Eleonora Giunchiglia, Anton Nemchenko, and Mihaela van der Schaar. RNN-SURV: A deep recurrent model for survival analysis. In *International conference on artificial neural networks*, pages 23–32. Springer, 2018.
- Erika Graf, Claudia Schmoor, Willi Sauerbrei, and Martin Schumacher. Assessment and comparison of prognostic classification schemes for survival data. *Statistics in medicine*, 18(17-18):2529–2545, 1999.
- Seong Kyu Han, Dongyeop Lee, Heetak Lee, Donghyo Kim, Heehwa G Son, Jae-Seong Yang, Seung-Jae V Lee, and Sanguk Kim. Oasis 2: online application for survival analysis 2 with features for the analysis of maximal lifespan and healthspan in aging research. *Oncotarget*, 7(35):56147, 2016.
- Kaiming He, Xiangyu Zhang, Shaoqing Ren, and Jian Sun. Delving deep into rectifiers: Surpassing human-level performance on imagenet classification. In *Proceedings of the IEEE international conference on computer vision*, pages 1026–1034, 2015.
- Kaiming He, Xiangyu Zhang, Shaoqing Ren, and Jian Sun. Deep residual learning for image recognition. In *Proceedings of the IEEE conference on computer vision and pattern recognition*, pages 770–778, 2016.
- Sergey Ioffe and Christian Szegedy. Batch normalization: Accelerating deep network training by reducing internal covariate shift. In *International conference on machine learning*, pages 448–456. PMLR, 2015.
- J.D. Kalbfleisch and R.L. Prentice. *The Statistical Analysis of Failure Time Data*. Wiley Series in Probability and Statistics. Wiley, 2011. ISBN 9781118031230. URL <https://books.google.de/books?id=BR4Kq-a1MIMC>.
- Edward L Kaplan and Paul Meier. Nonparametric estimation from incomplete observations. *Journal of the American statistical association*, 53(282):457–481, 1958.
- Jared L Katzman, Uri Shaham, Alexander Cloninger, Jonathan Bates, Tingting Jiang, and Yuval Kluger. DeepSurv: personalized treatment recommender system using a Cox proportional hazards deep neural network. *BMC medical research methodology*, 18(1):1–12, 2018.
- Diederik P Kingma and Jimmy Ba. Adam: A method for stochastic optimization. *arXiv preprint arXiv:1412.6980*, 2014.
- David G Kleinbaum, Mitchel Klein, et al. *Survival analysis: a self-learning text*, volume 3. Springer, 2012.

- Dehan Kong, Joseph G Ibrahim, Eunjee Lee, and Hongtu Zhu. Flcrm: Functional linear cox regression model. *Biometrics*, 74(1):109–117, 2018.
- Håvard Kvamme, Ørnulf Borgan, and Ida Scheel. Time-to-event prediction with neural networks and Cox regression. *arXiv preprint arXiv:1907.00825*, 2019.
- Chin-Diew Lai, DN Murthy, and Min Xie. Weibull distributions and their applications. In *Springer Handbooks*, pages 63–78. Springer, 2006.
- Bernhard Lang. Monotonic multi-layer perceptron networks as universal approximators. In *International conference on artificial neural networks*, pages 31–37. Springer, 2005.
- Changhee Lee, William Zame, Jinsung Yoon, and Mihaela Van Der Schaar. Deephit: A deep learning approach to survival analysis with competing risks. In *Proceedings of the AAAI conference on artificial intelligence*, volume 32, 2018.
- Eunjee Lee, Hongtu Zhu, Dehan Kong, Yalin Wang, Kelly Sullivan Giovanello, and Joseph G Ibrahim. Bflcrm: A bayesian functional linear cox regression model for predicting time to conversion to alzheimer’s disease. *The annals of applied statistics*, 9(4):2153, 2015.
- Stanley Lemeshow, Susanne May, and David W Hosmer Jr. *Applied survival analysis: regression modeling of time-to-event data*. John Wiley & Sons, 2011.
- Monica Nicolau, Arnold J Levine, and Gunnar Carlsson. Topology based data analysis identifies a subgroup of breast cancers with a unique mutational profile and excellent survival. *Proceedings of the National Academy of Sciences*, 108(17):7265–7270, 2011.
- R Kelley Pace and Ronald Barry. Sparse spatial autoregressions. *Statistics & Probability Letters*, 33(3):291–297, 1997.
- Adam Paszke, Sam Gross, Soumith Chintala, Gregory Chanan, Edward Yang, Zachary DeVito, Zeming Lin, Alban Desmaison, Luca Antiga, and Adam Lerer. Automatic differentiation in pytorch. -, 2017.
- Kan Ren, Jiarui Qin, Lei Zheng, Zhengyu Yang, Weinan Zhang, Lin Qiu, and Yong Yu. Deep recurrent survival analysis. In *Proceedings of the AAAI Conference on Artificial Intelligence*, volume 33, pages 4798–4805, 2019.
- David Rindt, Robert Hu, David Steinsaltz, and Dino Sejdinovic. Survival regression with proper scoring rules and monotonic neural networks. In *International Conference on Artificial Intelligence and Statistics*, pages 1190–1205. PMLR, 2022.
- Patrick Royston and Mahesh KB Parmar. Flexible parametric proportional-hazards and proportional-odds models for censored survival data, with application to prognostic modelling and estimation of treatment effects. *Statistics in medicine*, 21(15):2175–2197, 2002.
- Shibani Santurkar, Dimitris Tsipras, Andrew Ilyas, and Aleksander Madry. How does batch normalization help optimization? *Advances in neural information processing systems*, 31, 2018.

- Willi Sauerbrei and Patrick Royston. Building multivariable prognostic and diagnostic models: transformation of the predictors by using fractional polynomials. *Journal of the Royal Statistical Society: Series A (Statistics in Society)*, 162(1):71–94, 1999.
- Alan D Saul. *Gaussian process based approaches for survival analysis*. PhD thesis, University of Sheffield, 2016.
- Claudia Schmoor, Willi Sauerbrei, Gunter Bastert, Martin Schumacher, and German Breast Cancer Study Group. Role of isolated locoregional recurrence of breast cancer: results of four prospective studies. *Journal of Clinical Oncology*, 18(8):1696–1708, 2000.
- Patrick Schwab, Arash Mehrjou, Sonali Parbhoo, Leo Anthony Celi, Jürgen Hetzel, Markus Hofer, Bernhard Schölkopf, and Stefan Bauer. Real-time prediction of COVID-19 related mortality using electronic health records. *Nature communications*, 12(1):1–16, 2021.
- Ahmed H Shahin, Joseph Jacob, Daniel C Alexander, and David Barber. Survival Analysis for Idiopathic Pulmonary Fibrosis using CT Images and Incomplete Clinical Data. *arXiv preprint arXiv:2203.11391*, 2022.
- Raphael Edward Benjamin Sonabend. *A theoretical and methodological framework for machine learning in survival analysis: Enabling transparent and accessible predictive modelling on right-censored time-to-event data*. PhD thesis, UCL (University College London), 2021.
- Shiva Verma. Analog-Clocks dataset. <https://www.kaggle.com/datasets/shivajbd/analog-clocks>, 2019.
- Ping Wang, Yan Li, and Chandan K Reddy. Machine learning for survival analysis: A survey. *ACM Computing Surveys (CSUR)*, 51(6):1–36, 2019.
- Martin Wiegand, Sarah L Cowan, Claire S Waddington, David J Halsall, Victoria L Keevil, Brian DM Tom, Vince Taylor, Effrossyni Gkrania-Klotsas, Jacobus Preller, and Robert JB Goudie. Development and validation of a dynamic 48-hour in-hospital mortality risk stratification for COVID-19 in a UK teaching hospital: a retrospective cohort study. *medRxiv*, pages 2021–02, 2022.
- Guolei Yang, Ying Cai, and Chandan K Reddy. Spatio-temporal check-in time prediction with recurrent neural network based survival analysis. In *Proceedings of the Twenty-Seventh International Joint Conference on Artificial Intelligence*, 2018.
- Jae-Seong Yang, Hyun-Jun Nam, Mihwa Seo, Seong Kyu Han, Yonghwan Choi, Hong Gil Nam, Seung-Jae Lee, and Sanguk Kim. Oasis: online application for the survival analysis of lifespan assays performed in aging research. *PLoS one*, 6(8):e23525, 2011.
- William J Youden. Index for rating diagnostic tests. *Cancer*, 3(1):32–35, 1950.
- Yunwei Zhang, Germaine Wong, Graham Mann, Samuel Muller, and Jean YH Yang. SurvBenchmark: comprehensive benchmarking study of survival analysis methods using both omics data and clinical data. *GigaScience*, 11, 2022.

Chenyang Zhong and Robert Tibshirani. Survival analysis as a classification problem. *arXiv preprint arXiv:1909.11171*, 2019.

Appendix A. The MONDE and SuMo networks

We begin with the MONDE network Chilinski and Silva (2020), which allows one to parameterize a mapping

$$M : \mathbb{R}^m \ni z \mapsto M(z) \in \mathbb{R} \quad (32)$$

that is guaranteed to be monotonically increasing. It is a feed-forward neural network with each layer being of the form

$$z_{k+1} = \varphi_k(W_k z_k). \quad (33)$$

Here $z_0 = z$ and W_k is an affine map with the weights of the linear part constrained to be non-negative. For the last layer, outputting a scalar, they set $\varphi_K = \text{id}$, otherwise $\varphi_k = \tanh$.

The SuMo network Rindt et al. (2022) consists of MONDE and a feature-extracting network

$$Q : \mathbb{R}^n \ni x \mapsto Q(x) \in \mathbb{R}^k \quad (34)$$

combined with

$$\mathcal{S} : \mathbb{R} \times \mathbb{R}^n \mapsto [0, 1] \quad (35)$$

to give

$$\mathcal{S}(t, x) = 1 - \text{sigmoid}(M([t, Q(x)])) . \quad (36)$$

Here $[t, Q(x)]$ denotes the concatenation of t and $Q(x)$. As M and the sigmoid function are monotonically increasing, the SuMo network, $\mathcal{S}(t, x)$, is monotonically decreasing in t .

As discussed in Rindt et al. (2022); Chilinski and Silva (2020), the SuMo network is not only monotonically decreasing but is also a universal approximator of survival curves. However, as there is no guarantee that $\mathcal{S}(0, x) = 1$ for all $x \in \mathbb{R}^n$, it does not necessarily produce survival curves. Note, for the SuMo model, $\mathcal{S}(0, x) = 1$ is even impossible, as $\text{sigmoid}(\cdot) > 0$.

Appendix B. Initialization of MONDE and MONDE+

We used Optuna Akiba et al. (2019) to run 1,000 hyperparameter optimization steps on the task in Section 5.1 to optimize the scale and sign of the random initializations of MONDE and MONDE+. This was motivated by the initialization’s strong influence demonstrated by the histograms in Figure 3.

B.1 Default MONDE initialization

Following Rindt et al. (2022), the default MONDE initialization initializes both the weight matrix and the bias with Gaussian noise with mean zero. The standard deviation used in the initial Gaussian noise for the weight matrix is $\sqrt{\text{input size}}$ and for the biases $\sqrt{\text{output size}}$ is used.

B.2 Hyperparameter optimization for MONDE

Here we take the absolute value of the default weights described above and scale them by a factor from the interval $[-10, 10]$. Performing 1000 hyperparameter optimization steps yields the factor 4.6 for the matrix and 6.6 for the bias.

The hyperparameter objective function was given by the maximum loss of three training runs, as described in Section 5.1. We took the maximum loss of three runs in the hope of improving the robustness to “unlucky” initializations, as shown by the histograms in Figure 3.

B.3 Hyperparameter optimization for MONDE+

For the convenience of the reader, we recall the definition of a MONDE+ layer to be

$$z_{k+1}(t, z_k, z_0) = H_k z_k + \sigma_k(\tilde{z}_k(t, z_k) + B_k z_k + L_k z_0) \quad (37)$$

with

$$\tilde{z}_k(t, z_k) = A_k (\phi_k(a_k t + b_k) \circ \psi_k(G_k z_k)) \quad (38)$$

where the capital letters denote affine maps and \circ denotes the Hadamard product.

For simplicity we initialized $a_k \in \mathbb{R}^{64}$ with the uniform distribution between 0 and 1 and $b_k \in \mathbb{R}^{64}$ to be zero.

The initialization of all matrices and biases in the affine maps was optimized before training the models. We first initialized with the Kaiming uniform initialization He et al. (2015) as implemented by PyTorch Paszke et al. (2017). With the exception of L_k , we took their absolute values and scaled them by a factor (the hyperparameter) between $[0, 10]$, as these matrices had to be non-negative.

As in the MONDE case, we also scaled the biases as purely non-negative or non-positive. We did so to mediate the following effect. Some of the matrices need to be non-negative, which, as we found, can lead to impaired training performance. This is likely due to a substantial distribution shift in the activations over the course of multiple layers making the optimization landscape less smooth Ioffe and Szegedy (2015); Santurkar et al. (2018). It seems that having accordingly biased biases can counter this effect to some degree.

We again optimized the same hyperparameter objective as in the MONDE case above for 1000 optimization steps. For simplicity, we optimized the factors of the matrices of all affine mappings as one, which yielded the scaling factor 0.2. The resulting factors for the biases were -8.5 for B_k , 10 for G_k , the bias of H_k given by the Kaiming initialization was used, and for A_k we removed the bias entirely, as it would be redundant.

Appendix C. Proof of Lemma 1

As the concatenation of monotonically increasing functions is monotonically increasing, it suffices to prove the monotonicity of a single layer.

We will prove monotonicity in t by showing that the derivative of the output of a layer

$$z_{k+1}(t, z_k, z_0) = H_k z_k + \sigma_k(\tilde{z}_k(t, z_k) + B_k z_k + L_k z_0) \quad (39)$$

is positive in t and z_k .

First, we have that

$$\begin{aligned}
 \partial_t \tilde{z}_k(t, z_k) &= \bar{A}_k \partial_t [\phi_k(a_k t + b_k) \circ \psi_k(G_k z_k)] \\
 &= \bar{A}_k \{ \partial_t [\phi_k(a_k t + b_k)] \circ \psi_k(G_k z_k) \\
 &\quad + \phi_k(a_k t + b_k) \circ \partial_t [\psi_k(G_k z_k)] \} \\
 &= \bar{A}_k \{ [\nabla \phi_k](a_k t + b_k) \circ a_k \circ \psi_k(G_k z_k) \\
 &\quad + \phi_k(a_k t + b_k) \circ \partial_t [\psi_k(G_k z_k)] \} \\
 &= \bar{A}_k \{ [\nabla \phi_k](a_k t + b_k) \circ a_k \circ \psi_k(G_k z_k) \\
 &\quad + \phi_k(a_k t + b_k) \circ [\partial_t \psi_k](G_k z_k) \circ \bar{G}_k \partial_t z_k \}
 \end{aligned} \tag{40}$$

and

$$\begin{aligned}
 \partial_{z_k} \tilde{z}_k(t, z_k) &= \bar{A}_k \partial_{z_k} [\phi_k(a_k t + b_k) \circ \psi_k(G_k z_k)] \\
 &= \bar{A}_k [\phi_k(a_k t + b_k) \circ \partial_{z_k} [\psi_k(G_k z_k)] \\
 &= \bar{A}_k [D\{\phi_k(a_k t + b_k)\} D\{(\nabla \psi_k)(G_k z_k)\} \bar{G}_k]
 \end{aligned} \tag{41}$$

where $D\{c\}$ denotes the diagonal matrix associated with a vector c . Also, \bar{A}_k and \bar{G}_k are the linear parts of the affine operators A_k and G_k respectively. As they only have non-negative weights in their linear parts and the non-linearities, ϕ_k , and ψ_k , are non-negative and monotonically increasing, both derivatives are pointwise non-negative.

Using this, we can compute the corresponding derivatives of z_k . We have

$$\begin{aligned}
 \partial_t z_{k+1}(t, z_k, z_0) &= H_k \partial_t z_k + (\nabla \sigma_k)(\tilde{z}_k(t, z_k) \\
 &\quad + B_k z_k + L_k z_0) \circ (\partial_t \tilde{z}_k(t, z_k) + B_k \partial_t z_k)
 \end{aligned} \tag{42}$$

and

$$\begin{aligned}
 \partial_{z_k} z_{k+1}(t, z_k, z_0) &= H_k + D\{(\nabla \sigma_k)(\tilde{z}_k(t, z_k) \\
 &\quad + B_k z_k + L_k z_0)\} (\partial_{z_k} \tilde{z}_k(t, z_k) + B_k).
 \end{aligned} \tag{43}$$

For the same reasons as above, every term in these expressions is pointwise non-negative. \square

Appendix D. Proof of Lemma 2

We begin by proving the first two points. As $\alpha(t, x), \Lambda_0(t) \geq 0$ for all $(t, x) \in \mathbb{R}_{\geq 0} \times \mathbb{R}^n$, it follows that $\mathcal{S}_{C^{\otimes x}}(t, x) \in [0, 1]$. Since $\Lambda_0(0) = 0$, we have the maxima $\mathcal{S}_{C^{\otimes x}}(0, x) = 1$.

We will now show that $\mathcal{S}_{C^{\otimes x}}$ is monotonically decreasing in t . As the β_i^\pm are monotonically increasing, the ω_i are monotonically increasing in t . Therefore α is monotonically increasing in t , which means $\alpha \Lambda_0$ is monotonically increasing in t and therefore $\mathcal{S}_{C^{\otimes x}}$ is monotonically decreasing in t .

The continuity in t of ω_i follows from the continuity of the functions involved. The minima at $\omega_i(0, x) = \beta_i^+(0)$ follows from the fact, that $\beta_i^-(0)$ and $\beta_i^+(0)$ are both monotonically increasing and $\beta^-(0) = \beta^+(0)$.

We will now prove the continuity of α in (t, x) . We can reduce this problem to the continuity of each separate

$$\omega_i(t, x)|x_i - o_i|. \quad (44)$$

As all functions involved are otherwise continuous, we only need to show continuity at $x_i = o_i$. Considering the limits of each of the two factors completes the proof. \square

Appendix E. Datasets and preprocessing

For the NKI dataset, we reduced the number of features to make it accessible to classical survival models and easier to handle in general. We did so by only retaining only 9 of the features with a high correlation with survival time and observed outcome. This left us with the features: NM_004701, NM_001168, NM_003430, grade, NM_003981, AL050227, NM_018410, NM_000779, and NM_001809.

We assembled the COVID-19 dataset from COVID-19 patient data from Addenbrooke’s hospital in Cambridge, UK. We used the data of all patients on the day of their first positive COVID-19 test. We then used the following features of that day: age, gender, DNA CPR, median ventilation score over 24 hours, SpO2, pulse, temperature, respiration, NEWS2 score, O2 flow rate, FiO2, weight, height, BMI, Glasgow coma scale score, and SpO2/FiO2 Wiegand et al. (2022). We used these variables either due to their ready availability or because they were shown to be useful in previous work Wiegand et al. (2022). We gathered their survival time via their death records. We assumed we had no censoring within the first 28 days and then marked all other patients as censored on the 28th day. Exact censoring was hard to perform, but the hospital transferred only a small number of ICU patients, therefore, we believe that for the analysis in this paper, censoring is a negligible problem in this datasets.

To avoid numerical problems for the classical models, we also divided the times of the GBSG2 and Lymph datasets by 100 and those of the Recur dataset by 10. Except for standardizing the mean and standard deviation to 0 and 1, respectively, we did not use any other preprocessing.

In addition to the original sources, one can find summaries of the Lymph, Recur, and GBSG2 datasets in the *lifelines* documentation Davidson-Pilon (2022).

Appendix F. Training details

F.1 Training

We used *lifelines* Davidson-Pilon (2022) to train the classical models, i.e. Kaplan-Meier Kaplan and Meier (1958), Log-Logistic Bennett (1983), Log-Normal Gamel and McLean (1994), Weibull Lai et al. (2006), and two Cox models Cox and Oakes (2018) (one based on a piecewise constant Crowley and Breslow (1984) and one on a spline Efron (1988); Royston and Parmar (2002) baseline.)

For all the neural network models, we trained these using *PyTorch* Paszke et al. (2017). As the network training is stochastic, we train each network setup five times and pick the best model based on the mean score over all evaluation metrics on the validation set. For the neural networks, we also compare our BCE loss from (9) with the survival loss from Rindt

et al. (2022), namely

$$L_{\text{SuMo}} = -[e \log f(t|x) + (1 - e) \log S(t|x)]. \quad (45)$$

For the convenience of the reader we recall $f = -\partial_t S(t|x)$. Following common practice, we will use a weighted version of the BCE in the BCE loss. To ensure fair comparability, we therefore introduce a hyperparameter $\gamma > 0$ in the SuMo loss defining

$$L_{\text{SuMo}}^\gamma = -[e\gamma \log f(t|x) + (1 - e) \log S(t|x)]. \quad (46)$$

For every dataset, except Clocks, we trained the networks CoxNN, C \odot xNN, CoxDeepNN, SuMo, SuMo+, and SuMo++. For the Clocks dataset, we train SuMo, SuMo+, and SuMo++ as well as the CoxDeepNNs with the convolutional feature network and the Kaplan-Meier model. The CoxNN is based on Section 4.1 and the C \odot xNN is based on Section 4.2. The CoxDeepNN is also based on Section 4.1, but the linear scalar product in (24) is replaced by a deep feature network as independently proposed by Katzman et al. (2018); Kvamme et al. (2019) and Shahin et al. (2022). For the exact architecture of the feature networks of the CoxDeepNN and SuMo, SuMo+, and SuMo++, see the following section.

During our numerical experiments, we found that the training of any Cox-like model via L_{SuMo} tends to diverge, especially if the training data is predominately non-censored. In those cases, the training with L_{BCE} tends to be more stable but occasionally also diverges. We could ameliorate these issues by employing weight decay for all Cox-like models during all trainings.

All hyperparameters and training details for the different datasets are detailed in appendix Section F.6.

F.2 SuMo’s, SuMo+’s, and SuMo++’s dense feature network

All feature networks are simple feed-forward networks. SuMo, SuMo+, and SuMo++ have three dense layers of width 32, each followed by a ReLU activation and a layer-normalization.

F.3 SuMo’s, SuMo+’s, and SuMo++’s convolutional feature network

In the convolutional setting, i.e., for the Clocks dataset, SuMo, SuMo+, and SuMo++ have three 2-dimensional convolution layers, each with 128 channels, a kernel size of 3, and a padding of 1. Each is followed by a max-pooling layer with a kernel size of 3, a stride of 2, and padding of 1. Each of these pooling layers is followed by a ReLU activation and a layer normalization. These three layer-blocks are followed by a dense layer of width 48, a ReLU, a layer-normalization, another dense layer of width 48, and a final ReLU.

F.4 CoxDeepNN’s dense feature network

The network begins with two dense layers, the first with a width of twice the number of input features, see Table 1 and the second with a width of 8. Each of the two layers is followed by a layer normalization and a ReLU. Finally, the last layer is a dense layer of width 1.

Dataset	γ	BCE weight	σ_{factor}	weight decay for SuMo	weight decay for BCE
GBSG2	2.70	0.71	0.82	0.005	0.020
Recur	0.87	0.85	0.96	0.001	0.001
NKI	5.47	0.97	0.98	0.000	0.000
Lymph	3.44	0.86	0.79	0.004	0.002
COVID	2.49	0.92	0.71	0.000	0.002
Clocks	9.39	0.91	0.26	0.000	0.000
California	0.89	0.53	0.50	0.009	0.005

Table 3: Results of the hyperparameter search.

F.5 CoxDeepNN’s convolutional feature network

This network is the same as the one in Section F.3, except that the exp function replaces the final ReLU layer.

F.6 Hyperparameters

For all networks, we use the Adam optimizer Kingma and Ba (2014) with a step-size of 10^{-3} , gradient clipping of 1, and batch size of 8. After each batch, we also evaluate the loss of a batch from the validation set. We stopped the training when the 512-moving average over these validation batches did not decrease for 8192 batches or after at most 200000 training steps. With the exception of the Clocks dataset, which we trained on an Nvidia GeForce GTX 1080 Ti, we trained all models on the CPU. Each training took approximately 5 to 90 minutes.

For each dataset, we optimized the following hyperparameters with Optuna Akiba et al. (2019) by evaluating the results of 100 short training runs, each only 1024 training steps long:

- γ for the L_{SuMo}^γ loss over $[0, 10]$.
- The BCE weight L_{BCE} loss over $[0, 1]$.
- The σ for the L_{BCE} loss indirectly via the factor $\sigma_{\text{factor}} \in [0, 1]$ and $\sigma = \sigma_{\text{factor}} T_{\text{max}}$.
- One joint weight decay parameter for all Cox-like models in the case of the L_{SuMo}^γ loss over $[0, 1]$ and a separate one for the L_{BCE} loss.

For the resulting parameters, see Figure 3. We employed the mean of the concordance index and all integrated scores, except the integrated Brier score, as the loss function. The integrated Brier score was incorporated at a later stage of the paper. We determined appropriate ranges for the hyperparameters through a series of preliminary experiments.

Appendix G. Further numerical results

Figure 3 shows how well SuMo, SuMo+, and SuMo++ can fit the data points of Figure 2. Figure 4 shows that both SuMo+ and SuMo++ benefit from further training steps until convergences after 2048 training steps. SuMo+ almost improves to the level of SuMo++ – while SuMo shows no significant improvement.

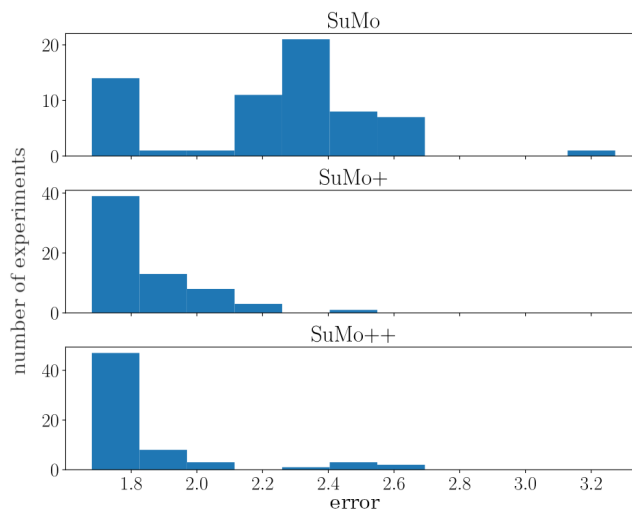


Figure 4: Analogous to Figure 3 but after convergence (2048 steps). SuMo did not improve over the 512 training steps. SuMo+ improved significantly but is still inferior to SuMo++.

Appendix H. Tables containing the separate scores

The Tables 4, 5, 6, 7, 9, 10, 11, 13, 14, 15, 16 show the separate integrated classifier metrics, and Figure 17 shows the inverted classical Brier score; we invert it so that for all of these metrics, we have that the large the better. Finally, Table 8 also presents the concordance index based on the mean survival time, and Table 12 presents the minimum of all of these scores for each model and dataset.

Model Loss-function	COVID-19	NKI	BGS2	Recur	Lymph	Clocks	California
Kaplan-Meier	0.56	0.56	0.65	0.76	0.54	0.73	0.74
Weibull	0.61	0.42	0.50	0.85	0.31	\emptyset	0.76
Log-logistic	0.58	0.42	0.49	0.85	0.34	\emptyset	0.76
Log-normal	0.58	0.42	0.50	0.85	0.35	\emptyset	0.76
Cox-piecewise	0.62	0.41	0.49	0.85	0.32	\emptyset	0.76
Cox-spline	0.61	0.42	0.49	0.85	0.31	\emptyset	0.76
CoxNN SuMo	0.59	0.46	0.49	0.84	0.35	\emptyset	0.76
CoxNN BCE	0.61	0.49	0.49	0.85	0.34	\emptyset	0.76
C \otimes xNN SuMo	0.60	0.46	0.48	0.85	0.35	\emptyset	0.75
C \otimes xNN BCE	0.59	0.40	0.51	0.85	0.35	\emptyset	0.70
CoxDeepNN SuMo	0.64	0.38	0.47	0.84	0.36	0.83	0.77
CoxDeepNN BCE	0.55	0.47	0.45	0.86	0.32	0.91	0.78
SuMo SuMo	0.55	0.40	0.37	0.86	0.31	0.99	0.84
SuMo BCE	0.53	0.50	0.47	0.86	0.28	0.96	0.83
SuMo+ SuMo	0.61	0.37	0.41	0.84	0.33	0.99	0.85
SuMo+ BCE	0.58	0.44	0.49	0.84	0.29	0.99	0.82
SuMo++ SuMo	0.56	0.44	0.46	0.85	0.31	0.98	0.85
SuMo++ BCE	0.55	0.53	0.55	0.83	0.37	0.94	0.83

Table 4: The over time integrated AUPRC for each model and dataset.

Model Loss-function	COVID-19	NKI	BGS2	Recur	Lymph	Clocks	California
Kaplan-Meier	0.50	0.55	0.50	0.50	0.55	0.50	0.50
Weibull	0.95	0.82	0.73	0.91	0.72	\emptyset	0.86
Log-logistic	0.95	0.82	0.72	0.91	0.74	\emptyset	0.88
Log-normal	0.95	0.82	0.72	0.91	0.75	\emptyset	0.87
Cox-piecewise	0.95	0.81	0.73	0.91	0.72	\emptyset	0.86
Cox-spline	0.95	0.81	0.73	0.91	0.72	\emptyset	0.86
CoxNN SuMo	0.95	0.83	0.70	0.90	0.75	\emptyset	0.87
CoxNN BCE	0.95	0.83	0.72	0.90	0.75	\emptyset	0.86
C \otimes xNN SuMo	0.94	0.81	0.71	0.91	0.76	\emptyset	0.81
C \otimes xNN BCE	0.95	0.82	0.71	0.91	0.75	\emptyset	0.81
CoxDeepNN SuMo	0.94	0.81	0.74	0.90	0.77	0.78	0.87
CoxDeepNN BCE	0.94	0.82	0.70	0.91	0.75	0.96	0.87
SuMo SuMo	0.94	0.78	0.63	0.91	0.75	0.99	0.92
SuMo BCE	0.93	0.83	0.72	0.91	0.72	0.98	0.93
SuMo+ SuMo	0.92	0.77	0.66	0.90	0.72	0.99	0.95
SuMo+ BCE	0.94	0.80	0.71	0.91	0.73	0.99	0.91
SuMo++ SuMo	0.91	0.80	0.72	0.91	0.74	0.99	0.94
SuMo++ BCE	0.88	0.86	0.74	0.89	0.74	0.97	0.93

Table 5: The over time integrated AUROC for each model and dataset.

Model Loss-function	COVID-19	NKI	BGS2	Recur	Lymph	Clocks	California
Kaplan-Meier	0.79	0.69	0.63	0.57	0.74	0.63	0.69
Weibull	0.90	0.76	0.67	0.77	0.76	\emptyset	0.80
Log-logistic	0.90	0.77	0.67	0.78	0.76	\emptyset	0.83
Log-normal	0.90	0.77	0.67	0.78	0.76	\emptyset	0.82
Cox-piecewise	0.90	0.76	0.67	0.77	0.76	\emptyset	0.80
Cox-spline	0.90	0.76	0.67	0.77	0.76	\emptyset	0.80
CoxNN SuMo	0.90	0.69	0.63	0.79	0.70	\emptyset	0.78
CoxNN BCE	0.86	0.60	0.66	0.74	0.67	\emptyset	0.70
C \otimes xNN SuMo	0.91	0.72	0.65	0.82	0.70	\emptyset	0.78
C \otimes xNN BCE	0.84	0.74	0.63	0.81	0.70	\emptyset	0.73
CoxDeepNN SuMo	0.91	0.73	0.64	0.81	0.78	0.86	0.78
CoxDeepNN BCE	0.87	0.66	0.64	0.80	0.72	0.87	0.71
SuMo SuMo	0.92	0.77	0.66	0.82	0.78	0.98	0.89
SuMo BCE	0.90	0.72	0.71	0.83	0.72	0.93	0.87
SuMo+ SuMo	0.91	0.76	0.67	0.81	0.75	0.98	0.89
SuMo+ BCE	0.90	0.75	0.71	0.80	0.74	0.94	0.88
SuMo++ SuMo	0.90	0.76	0.65	0.82	0.75	0.97	0.89
SuMo++ BCE	0.90	0.78	0.72	0.81	0.76	0.93	0.87

Table 6: The over time integrated accuracy score for each model and dataset.

Model Loss-function	COVID-19	NKI	BGS2	Recur	Lymph	Clocks	California
Kaplan-Meier	0.50	0.50	0.50	0.50	0.50	0.50	0.50
Weibull	0.69	0.56	0.55	0.72	0.54	\emptyset	0.64
Log-logistic	0.70	0.58	0.55	0.74	0.54	\emptyset	0.68
Log-normal	0.70	0.57	0.55	0.75	0.54	\emptyset	0.67
Cox-piecewise	0.69	0.57	0.55	0.73	0.54	\emptyset	0.64
Cox-spline	0.69	0.57	0.55	0.72	0.54	\emptyset	0.64
CoxNN SuMo	0.74	0.60	0.54	0.75	0.55	\emptyset	0.64
CoxNN BCE	0.81	0.59	0.55	0.69	0.55	\emptyset	0.60
C \otimes xNN SuMo	0.79	0.62	0.56	0.78	0.57	\emptyset	0.62
C \otimes xNN BCE	0.80	0.62	0.55	0.78	0.55	\emptyset	0.59
CoxDeepNN SuMo	0.78	0.59	0.59	0.77	0.56	0.72	0.65
CoxDeepNN BCE	0.82	0.65	0.53	0.77	0.57	0.81	0.61
SuMo SuMo	0.77	0.61	0.55	0.79	0.58	0.97	0.78
SuMo BCE	0.83	0.69	0.59	0.80	0.55	0.91	0.76
SuMo+ SuMo	0.77	0.57	0.56	0.79	0.57	0.96	0.79
SuMo+ BCE	0.86	0.66	0.59	0.78	0.57	0.90	0.77
SuMo++ SuMo	0.80	0.64	0.57	0.79	0.57	0.95	0.78
SuMo++ BCE	0.79	0.70	0.59	0.78	0.60	0.92	0.77

Table 7: The over time integrated balanced accuracy score for each model and dataset.

Model Loss-function	COVID-19	NKI	BGS2	Recur	Lymph	Clocks	California
Kaplan-Meier	0.50	0.50	0.50	0.50	0.50	0.50	0.50
Weibull	0.93	0.76	0.70	0.82	0.67	\emptyset	0.81
Log-logistic	0.93	0.76	0.69	0.82	0.68	\emptyset	0.82
Log-normal	0.93	0.76	0.69	0.82	0.69	\emptyset	0.81
Cox-piecewise	0.93	0.75	0.70	0.82	0.67	\emptyset	0.81
Cox-spline	0.93	0.75	0.70	0.82	0.67	\emptyset	0.81
CoxNN SuMo	0.93	0.77	0.67	0.82	0.70	\emptyset	0.82
CoxNN BCE	0.94	0.77	0.69	0.82	0.69	\emptyset	0.81
C \otimes xNN SuMo	0.93	0.75	0.68	0.82	0.71	\emptyset	0.78
C \otimes xNN BCE	0.93	0.76	0.67	0.83	0.70	\emptyset	0.75
CoxDeepNN SuMo	0.93	0.75	0.69	0.82	0.70	0.88	0.83
CoxDeepNN BCE	0.92	0.76	0.66	0.82	0.69	0.90	0.82
SuMo SuMo	0.92	0.71	0.60	0.82	0.68	0.97	0.87
SuMo BCE	0.92	0.75	0.69	0.82	0.65	0.92	0.86
SuMo+ SuMo	0.91	0.68	0.63	0.81	0.66	0.98	0.88
SuMo+ BCE	0.93	0.72	0.68	0.81	0.67	0.94	0.86
SuMo++ SuMo	0.90	0.71	0.67	0.81	0.67	0.96	0.88
SuMo++ BCE	0.87	0.79	0.69	0.80	0.69	0.91	0.86

Table 8: The concordance index based on the dataset’s restricted mean survival time for each model and dataset.

Model Loss-function	COVID-19	NKI	BGS2	Recur	Lymph	Clocks	California
Kaplan-Meier	0.12	0.21	0.30	0.53	0.17	0.48	0.48
Weibull	0.46	0.29	0.36	0.73	0.24	\emptyset	0.61
Log-logistic	0.48	0.31	0.37	0.74	0.25	\emptyset	0.65
Log-normal	0.48	0.31	0.37	0.75	0.25	\emptyset	0.64
Cox-piecewise	0.46	0.30	0.36	0.73	0.24	\emptyset	0.61
Cox-spline	0.46	0.30	0.36	0.73	0.24	\emptyset	0.61
CoxNN SuMo	0.52	0.37	0.39	0.76	0.30	\emptyset	0.62
CoxNN BCE	0.52	0.39	0.36	0.74	0.29	\emptyset	0.58
C \otimes xNN SuMo	0.58	0.39	0.40	0.77	0.31	\emptyset	0.60
C \otimes xNN BCE	0.49	0.39	0.39	0.78	0.28	\emptyset	0.58
CoxDeepNN SuMo	0.56	0.35	0.46	0.78	0.27	0.55	0.64
CoxDeepNN BCE	0.54	0.43	0.35	0.78	0.30	0.82	0.58
SuMo SuMo	0.58	0.38	0.39	0.78	0.31	0.97	0.75
SuMo BCE	0.59	0.49	0.39	0.81	0.28	0.88	0.72
SuMo+ SuMo	0.55	0.30	0.40	0.77	0.31	0.96	0.76
SuMo+ BCE	0.61	0.45	0.39	0.79	0.29	0.89	0.73
SuMo++ SuMo	0.57	0.42	0.44	0.78	0.29	0.94	0.75
SuMo++ BCE	0.57	0.50	0.40	0.80	0.33	0.88	0.72

Table 9: The over time integrated F_1 score for each model and dataset.

Model Loss-function	COVID-19	NKI	BGS2	Recur	Lymph	Clocks	California
Kaplan-Meier	0.12	0.21	0.30	0.52	0.17	0.49	0.48
Weibull	0.44	0.27	0.36	0.74	0.24	\emptyset	0.62
Log-logistic	0.46	0.29	0.37	0.76	0.24	\emptyset	0.66
Log-normal	0.47	0.29	0.36	0.76	0.25	\emptyset	0.64
Cox-piecewise	0.44	0.28	0.36	0.74	0.24	\emptyset	0.62
Cox-spline	0.44	0.28	0.36	0.74	0.24	\emptyset	0.62
CoxNN SuMo	0.53	0.44	0.43	0.78	0.35	\emptyset	0.65
CoxNN BCE	0.63	0.51	0.35	0.81	0.36	\emptyset	0.62
C \otimes xNN SuMo	0.62	0.45	0.44	0.78	0.37	\emptyset	0.62
C \otimes xNN BCE	0.62	0.43	0.42	0.82	0.33	\emptyset	0.61
CoxDeepNN SuMo	0.60	0.38	0.54	0.80	0.26	0.55	0.70
CoxDeepNN BCE	0.65	0.55	0.36	0.83	0.33	0.88	0.62
SuMo SuMo	0.58	0.39	0.43	0.80	0.33	0.96	0.74
SuMo BCE	0.67	0.57	0.37	0.85	0.30	0.92	0.73
SuMo+ SuMo	0.58	0.28	0.41	0.76	0.34	0.95	0.76
SuMo+ BCE	0.70	0.50	0.36	0.83	0.31	0.93	0.75
SuMo++ SuMo	0.63	0.46	0.50	0.79	0.31	0.94	0.75
SuMo++ BCE	0.61	0.55	0.37	0.84	0.36	0.92	0.73

Table 10: The over time integrated F_2 score for each model and dataset.

Model Loss-function	COVID-19	NKI	BGS2	Recur	Lymph	Clocks	California
Kaplan-Meier	0.12	0.21	0.30	0.53	0.18	0.47	0.48
Weibull	0.48	0.32	0.36	0.71	0.25	\emptyset	0.60
Log-logistic	0.50	0.33	0.37	0.73	0.25	\emptyset	0.65
Log-normal	0.50	0.34	0.37	0.73	0.26	\emptyset	0.64
Cox-piecewise	0.49	0.32	0.36	0.72	0.25	\emptyset	0.60
Cox-spline	0.49	0.32	0.36	0.72	0.25	\emptyset	0.60
CoxNN SuMo	0.50	0.33	0.36	0.74	0.26	\emptyset	0.59
CoxNN BCE	0.45	0.31	0.36	0.69	0.25	\emptyset	0.55
C \otimes xNN SuMo	0.55	0.35	0.37	0.77	0.27	\emptyset	0.58
C \otimes xNN BCE	0.41	0.36	0.37	0.75	0.25	\emptyset	0.55
CoxDeepNN SuMo	0.54	0.33	0.41	0.76	0.28	0.55	0.60
CoxDeepNN BCE	0.47	0.36	0.35	0.74	0.27	0.77	0.56
SuMo SuMo	0.58	0.37	0.37	0.77	0.29	0.97	0.75
SuMo BCE	0.54	0.44	0.42	0.78	0.26	0.85	0.71
SuMo+ SuMo	0.53	0.32	0.38	0.78	0.29	0.97	0.75
SuMo+ BCE	0.54	0.41	0.43	0.75	0.27	0.86	0.72
SuMo++ SuMo	0.53	0.39	0.40	0.77	0.28	0.94	0.75
SuMo++ BCE	0.55	0.47	0.43	0.76	0.31	0.85	0.71

Table 11: The over time integrated $F_{0.5}$ score for each model and dataset.

Model Loss-function	COVID-19	NKI	BGS2	Recur	Lymph	Clocks	California
Kaplan-Meier	0.00	0.00	0.00	0.00	0.00	0.00	0.00
Weibull	0.38	0.13	0.10	0.44	0.08	\emptyset	0.29
Log-logistic	0.40	0.16	0.10	0.49	0.08	\emptyset	0.36
Log-normal	0.41	0.15	0.10	0.49	0.09	\emptyset	0.33
Cox-piecewise	0.38	0.14	0.10	0.45	0.08	\emptyset	0.28
Cox-spline	0.38	0.13	0.10	0.45	0.08	\emptyset	0.28
CoxNN SuMo	0.48	0.21	0.09	0.50	0.12	\emptyset	0.29
CoxNN BCE	0.41	0.22	0.09	0.39	0.12	\emptyset	0.20
C \otimes xNN SuMo	0.53	0.24	0.11	0.57	0.14	\emptyset	0.24
C \otimes xNN BCE	0.37	0.25	0.09	0.56	0.11	\emptyset	0.17
CoxDeepNN SuMo	0.52	0.19	0.19	0.55	0.13	0.44	0.31
CoxDeepNN BCE	0.43	0.32	0.07	0.54	0.15	0.63	0.22
SuMo SuMo	0.54	0.25	0.10	0.58	0.16	0.94	0.56
SuMo BCE	0.51	0.41	0.18	0.60	0.13	0.82	0.51
SuMo+ SuMo	0.52	0.17	0.12	0.57	0.15	0.92	0.59
SuMo+ BCE	0.51	0.35	0.18	0.56	0.14	0.81	0.53
SuMo++ SuMo	0.50	0.30	0.15	0.58	0.14	0.90	0.57
SuMo++ BCE	0.54	0.44	0.19	0.57	0.20	0.83	0.54

Table 12: The minimum of all over time integrated scores for each model and dataset.

Model Loss-function	COVID-19	NKI	BGS2	Recur	Lymph	Clocks	California
Kaplan-Meier	0.12	0.21	0.30	0.53	0.19	0.47	0.48
Weibull	0.50	0.33	0.37	0.71	0.25	\emptyset	0.60
Log-logistic	0.51	0.35	0.37	0.73	0.26	\emptyset	0.65
Log-normal	0.51	0.36	0.37	0.73	0.26	\emptyset	0.64
Cox-piecewise	0.50	0.33	0.37	0.71	0.25	\emptyset	0.60
Cox-spline	0.51	0.33	0.37	0.71	0.25	\emptyset	0.60
CoxNN SuMo	0.49	0.30	0.34	0.72	0.24	\emptyset	0.58
CoxNN BCE	0.41	0.27	0.36	0.65	0.23	\emptyset	0.54
C \otimes xNN SuMo	0.53	0.32	0.36	0.77	0.25	\emptyset	0.57
C \otimes xNN BCE	0.37	0.34	0.35	0.73	0.23	\emptyset	0.54
CoxDeepNN SuMo	0.52	0.32	0.38	0.75	0.29	0.56	0.57
CoxDeepNN BCE	0.43	0.32	0.35	0.72	0.26	0.74	0.55
SuMo SuMo	0.58	0.36	0.36	0.76	0.29	0.97	0.76
SuMo BCE	0.51	0.41	0.45	0.76	0.25	0.84	0.70
SuMo+ SuMo	0.52	0.33	0.38	0.78	0.28	0.98	0.75
SuMo+ BCE	0.51	0.39	0.45	0.73	0.26	0.85	0.71
SuMo++ SuMo	0.50	0.37	0.37	0.77	0.27	0.94	0.75
SuMo++ BCE	0.54	0.45	0.46	0.74	0.30	0.83	0.70

Table 13: The over time integrated precision score for each model and dataset.

Model Loss-function	COVID-19	NKI	BGS2	Recur	Lymph	Clocks	California
Kaplan-Meier	0.12	0.21	0.29	0.52	0.16	0.50	0.48
Weibull	0.43	0.26	0.35	0.75	0.23	\emptyset	0.62
Log-logistic	0.45	0.28	0.37	0.77	0.24	\emptyset	0.66
Log-normal	0.46	0.27	0.36	0.77	0.24	\emptyset	0.64
Cox-piecewise	0.43	0.27	0.36	0.75	0.24	\emptyset	0.63
Cox-spline	0.43	0.27	0.37	0.75	0.24	\emptyset	0.62
CoxNN SuMo	0.55	0.50	0.47	0.80	0.40	\emptyset	0.69
CoxNN BCE	0.75	0.65	0.35	0.86	0.42	\emptyset	0.68
C \otimes xNN SuMo	0.65	0.50	0.47	0.78	0.42	\emptyset	0.63
C \otimes xNN BCE	0.76	0.46	0.45	0.84	0.37	\emptyset	0.65
CoxDeepNN SuMo	0.63	0.41	0.61	0.81	0.26	0.55	0.76
CoxDeepNN BCE	0.77	0.69	0.36	0.86	0.36	0.93	0.69
SuMo SuMo	0.58	0.40	0.46	0.81	0.34	0.96	0.74
SuMo BCE	0.74	0.67	0.36	0.88	0.33	0.95	0.74
SuMo+ SuMo	0.60	0.27	0.43	0.75	0.37	0.94	0.76
SuMo+ BCE	0.81	0.55	0.35	0.86	0.34	0.97	0.76
SuMo++ SuMo	0.69	0.49	0.55	0.80	0.33	0.94	0.75
SuMo++ BCE	0.65	0.60	0.36	0.87	0.39	0.96	0.74

Table 14: The over time integrated sensitivity score for each model and dataset.

Model Loss-function	COVID-19	NKI	BGS2	Recur	Lymph	Clocks	California
Kaplan-Meier	0.88	0.79	0.71	0.48	0.84	0.50	0.52
Weibull	0.95	0.87	0.74	0.69	0.84	\emptyset	0.67
Log-logistic	0.95	0.87	0.74	0.72	0.85	\emptyset	0.70
Log-normal	0.95	0.88	0.74	0.72	0.85	\emptyset	0.69
Cox-piecewise	0.95	0.86	0.73	0.71	0.84	\emptyset	0.65
Cox-spline	0.95	0.86	0.73	0.70	0.84	\emptyset	0.66
CoxNN SuMo	0.93	0.69	0.62	0.70	0.71	\emptyset	0.60
CoxNN BCE	0.87	0.54	0.74	0.52	0.69	\emptyset	0.52
C \otimes xNN SuMo	0.93	0.73	0.65	0.78	0.71	\emptyset	0.60
C \otimes xNN BCE	0.84	0.77	0.65	0.72	0.73	\emptyset	0.52
CoxDeepNN SuMo	0.93	0.77	0.58	0.73	0.87	0.89	0.54
CoxDeepNN BCE	0.88	0.61	0.71	0.68	0.77	0.70	0.53
SuMo SuMo	0.96	0.83	0.64	0.76	0.81	0.98	0.83
SuMo BCE	0.92	0.72	0.82	0.72	0.78	0.86	0.77
SuMo+ SuMo	0.94	0.86	0.69	0.82	0.78	0.98	0.83
SuMo+ BCE	0.90	0.77	0.83	0.70	0.79	0.83	0.78
SuMo++ SuMo	0.92	0.79	0.60	0.78	0.80	0.96	0.82
SuMo++ BCE	0.93	0.81	0.83	0.70	0.80	0.88	0.79

Table 15: The over time integrated specificity score for each model and dataset.

Model Loss-function	COVID-19	NKI	BGS2	Recur	Lymph	Clocks	California
Kaplan-Meier	0.00	0.00	0.00	0.00	0.00	0.00	0.00
Weibull	0.38	0.13	0.10	0.44	0.08	\emptyset	0.29
Log-logistic	0.40	0.16	0.10	0.49	0.08	\emptyset	0.36
Log-normal	0.41	0.15	0.10	0.49	0.09	\emptyset	0.33
Cox-piecewise	0.38	0.14	0.10	0.45	0.08	\emptyset	0.28
Cox-spline	0.38	0.13	0.10	0.45	0.08	\emptyset	0.28
CoxNN SuMo	0.48	0.21	0.09	0.50	0.12	\emptyset	0.29
CoxNN BCE	0.62	0.22	0.09	0.39	0.12	\emptyset	0.20
C \otimes xNN SuMo	0.58	0.24	0.11	0.57	0.14	\emptyset	0.24
C \otimes xNN BCE	0.60	0.25	0.09	0.56	0.11	\emptyset	0.17
CoxDeepNN SuMo	0.56	0.19	0.19	0.55	0.13	0.44	0.31
CoxDeepNN BCE	0.64	0.34	0.07	0.54	0.15	0.63	0.22
SuMo SuMo	0.54	0.25	0.10	0.58	0.16	0.94	0.56
SuMo BCE	0.65	0.46	0.18	0.60	0.13	0.82	0.51
SuMo+ SuMo	0.54	0.17	0.12	0.57	0.15	0.92	0.59
SuMo+ BCE	0.72	0.35	0.18	0.56	0.14	0.81	0.53
SuMo++ SuMo	0.61	0.30	0.15	0.58	0.14	0.90	0.57
SuMo++ BCE	0.58	0.44	0.19	0.57	0.20	0.83	0.54

Table 16: The over time integrated Youden’s index for each model and dataset.

Model Loss-function	COVID-19	NKI	BGS2	Recur	Lymph	Clocks	California
Kaplan-Meier	0.90	0.84	0.81	0.78	0.86	0.81	0.85
Weibull	0.94	0.87	0.83	0.89	0.87	\emptyset	0.91
Log-logistic	0.94	0.87	0.84	0.89	0.87	\emptyset	0.92
Log-normal	0.94	0.87	0.83	0.89	0.88	\emptyset	0.91
Cox-piecewise	0.94	0.87	0.84	0.89	0.87	\emptyset	0.91
Cox-spline	0.94	0.87	0.84	0.89	0.87	\emptyset	0.91
CoxNN SuMo	0.95	0.85	0.82	0.89	0.85	\emptyset	0.90
CoxNN BCE	0.93	0.78	0.83	0.85	0.85	\emptyset	0.87
C \otimes xNN SuMo	0.94	0.85	0.82	0.90	0.85	\emptyset	0.89
C \otimes xNN BCE	0.93	0.86	0.83	0.89	0.86	\emptyset	0.88
CoxDeepNN SuMo	0.94	0.85	0.80	0.89	0.88	0.88	0.91
CoxDeepNN BCE	0.92	0.80	0.83	0.89	0.87	0.93	0.88
SuMo SuMo	0.94	0.82	0.77	0.90	0.84	0.98	0.94
SuMo BCE	0.92	0.75	0.82	0.88	0.83	0.96	0.93
SuMo+ SuMo	0.94	0.81	0.79	0.89	0.83	0.99	0.94
SuMo+ BCE	0.92	0.81	0.81	0.89	0.85	0.96	0.93
SuMo++ SuMo	0.94	0.83	0.79	0.90	0.85	0.98	0.95
SuMo++ BCE	0.92	0.84	0.83	0.88	0.84	0.96	0.93

 Table 17: The over time integrated inverted mean squared error defined as $1 - \text{MSE}$ for each model and dataset, I.e., $1 - \text{IBS}$ where IBS is the integrated Brier score.

Appendix I. Comparison of non-integrated balanced accuracy and F1 scores using plots

Here we provide the Figures 5, 6, 7, 8, 9, 10, 11. Each presents the non-integrated versions of the balanced accuracy and the F_1 score for the most prominent models – one figure for each dataset. We chose these two scores as they are highly correlated with the mean of the scores and seem to complement each other.

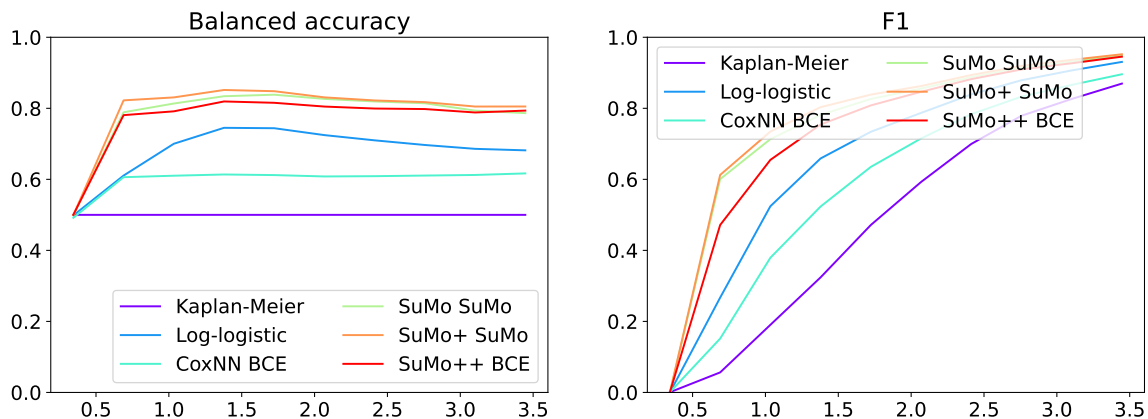


Figure 5: The balanced accuracy and the F_1 score over time for the California dataset.

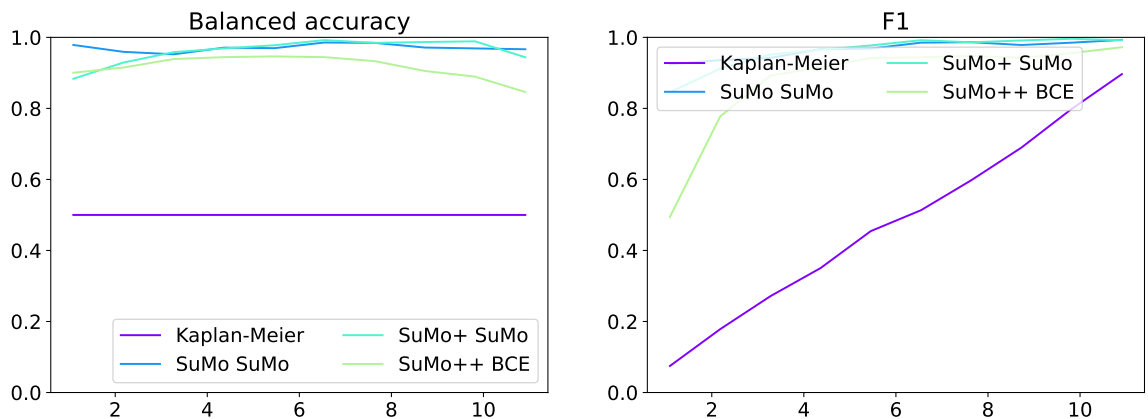


Figure 6: The balanced accuracy and the F_1 score over time for the Clocks dataset.

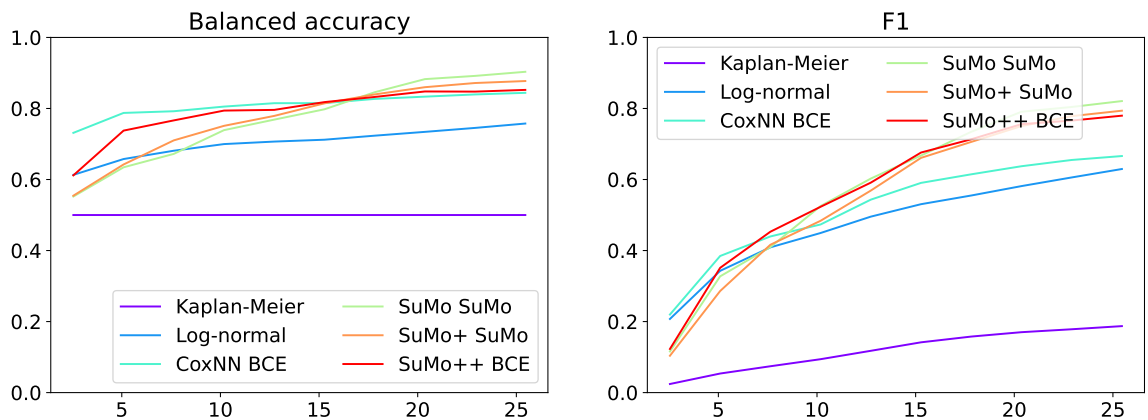


Figure 7: The balanced accuracy and the F_1 score over time for the COVID-19 dataset.

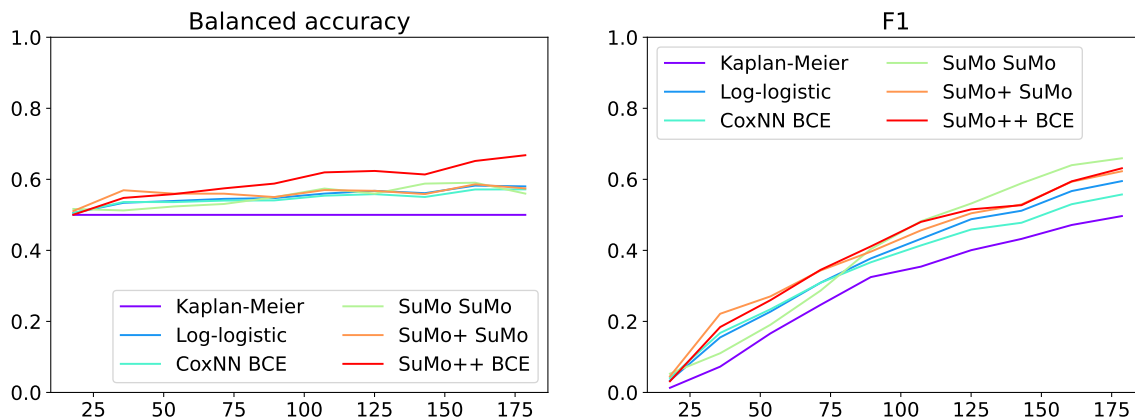


Figure 8: The balanced accuracy and the F_1 score over time for the GBSG2 dataset.

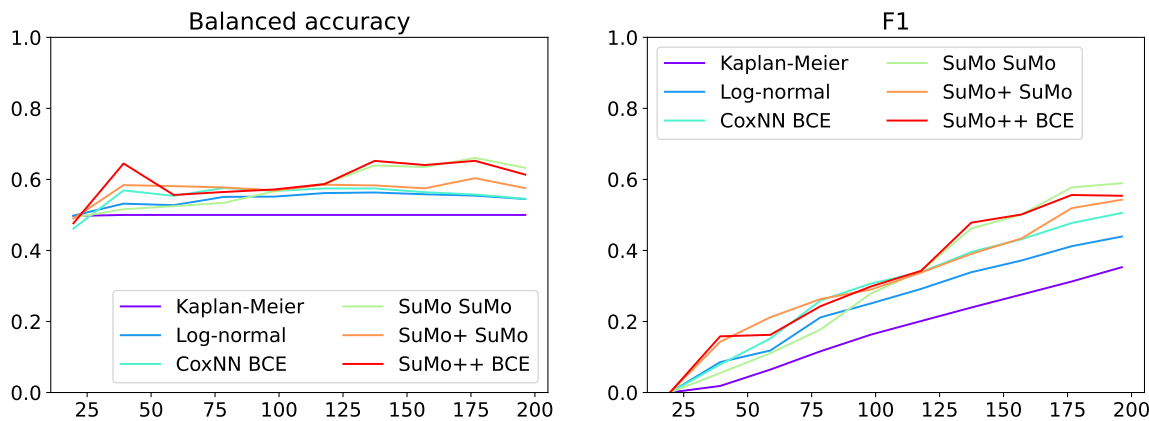


Figure 9: The balanced accuracy and the F_1 score over time for the Lymph dataset.

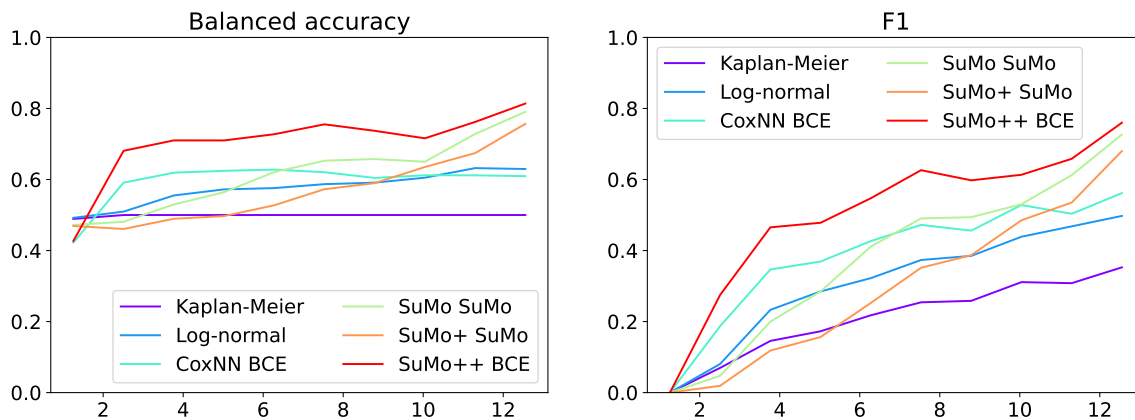


Figure 10: The balanced accuracy and the F_1 score over time for the NKI dataset.

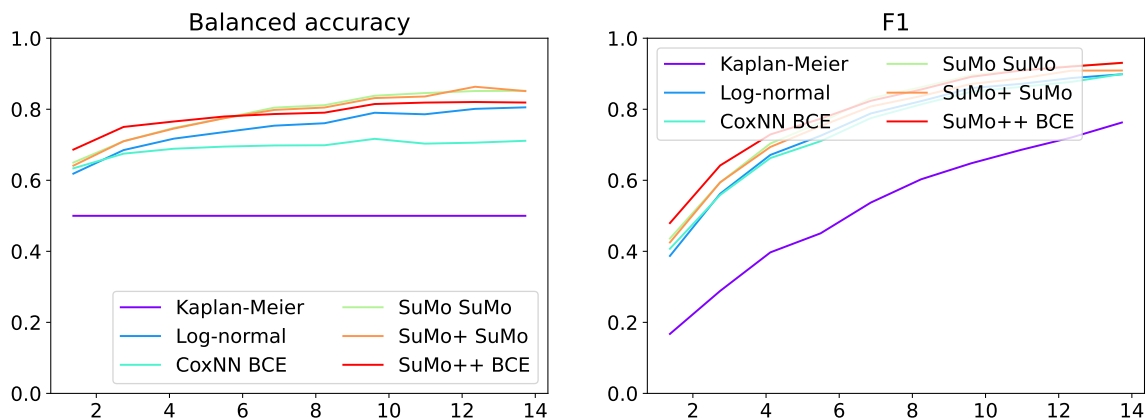


Figure 11: The balanced accuracy and the F_1 score over time for the Recur dataset.

Appendix J. Example plots of predicted survival curves

For the sake of readability, the Figures 12, 13, 14, 15, 16, 17, 18, 19, 20, 21, 22, 23, 24, 25 only show a selection of the trained models. For the classical models, we only select the one with the highest score in Table 2.

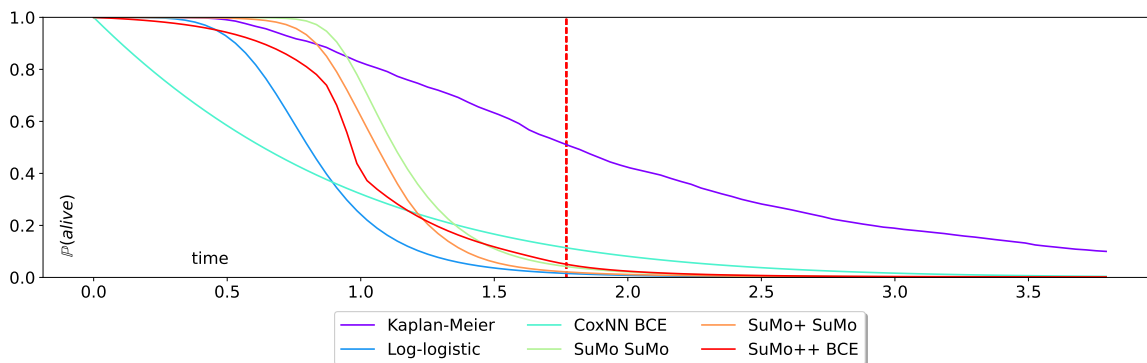


Figure 12: Survival curve examples for a sample from the California dataset up until T_{max} . The vertical line marks the time of the event or censoring (red: death, blue: censoring). The legend shows the model and, if applicable, the loss function (SuMo or BCE).

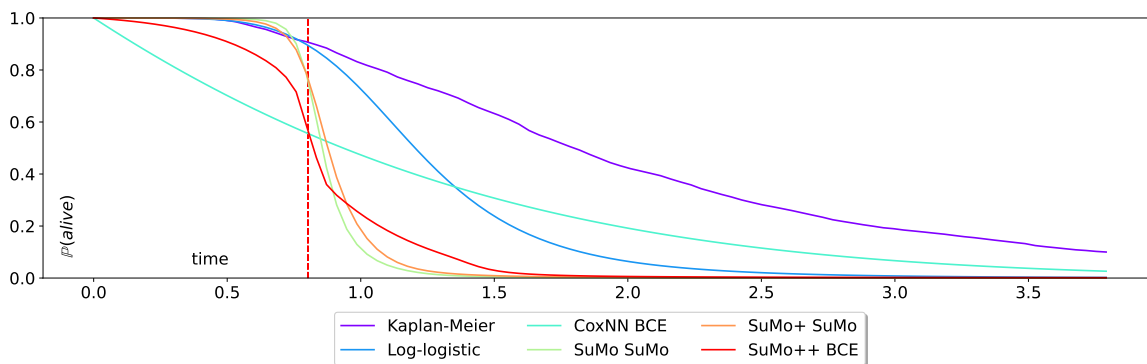


Figure 13: Survival curve examples for a sample from the California dataset up until T_{max} . The vertical line marks the time of the event or censoring (red: death, blue: censoring). The legend shows the model and, if applicable, the loss function (SuMo or BCE).

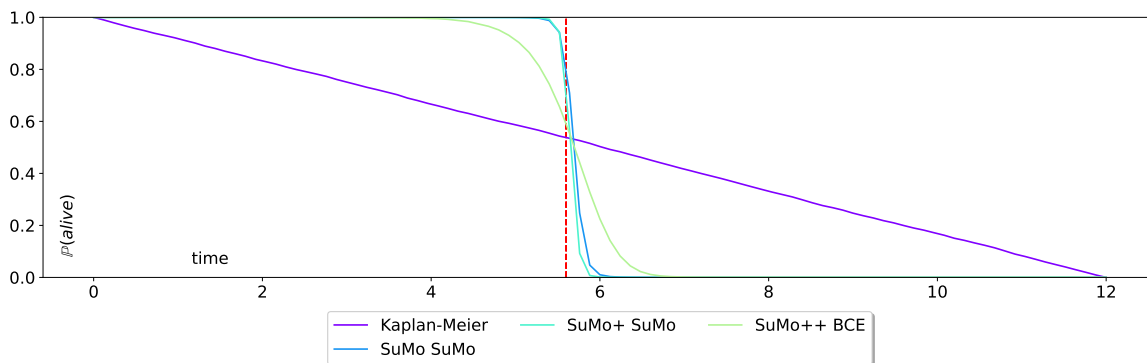


Figure 14: Survival curve examples for a sample from the Clocks dataset up until T_{max} . The vertical line marks the time of the event or censoring (red: death, blue: censoring). The legend shows the model and, if applicable, the loss function (SuMo or BCE).

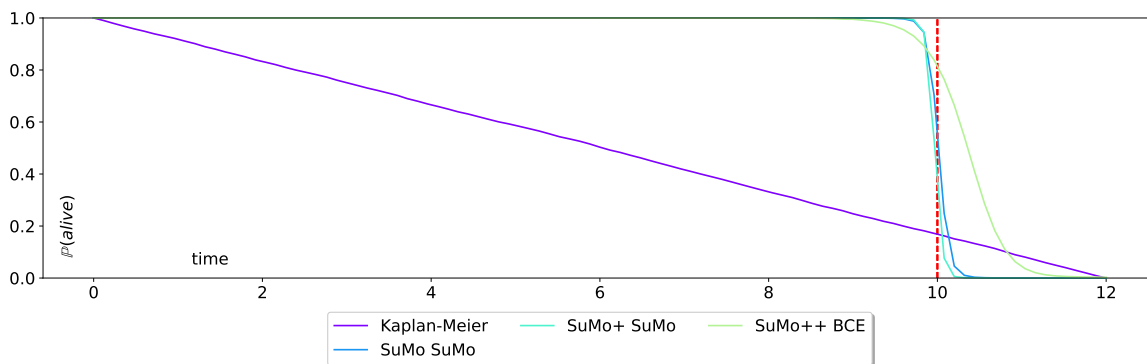


Figure 15: Survival curve examples for a sample from the Clocks dataset up until T_{max} . The vertical line marks the time of the event or censoring (red: death, blue: censoring). The legend shows the model and, if applicable, the loss function (SuMo or BCE).

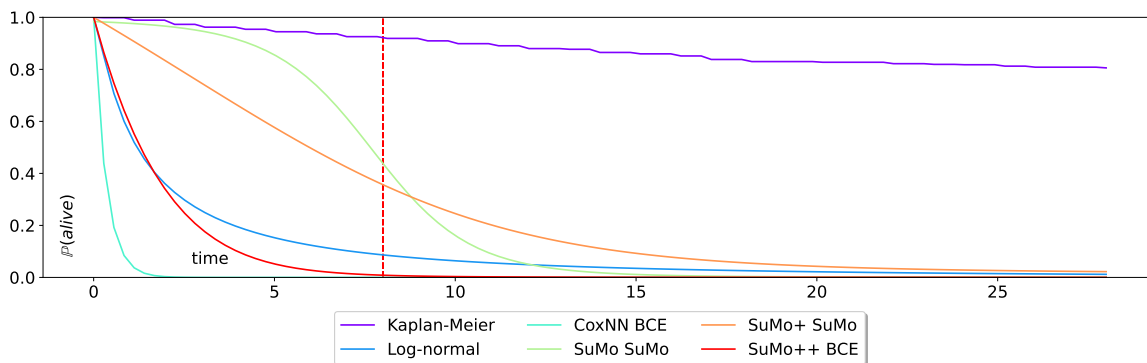


Figure 16: Survival curve examples for a sample from the COVID dataset up until T_{max} . The vertical line marks the time of the event or censoring (red: death, blue: censoring). The legend shows the model and, if applicable, the loss function (SuMo or BCE).

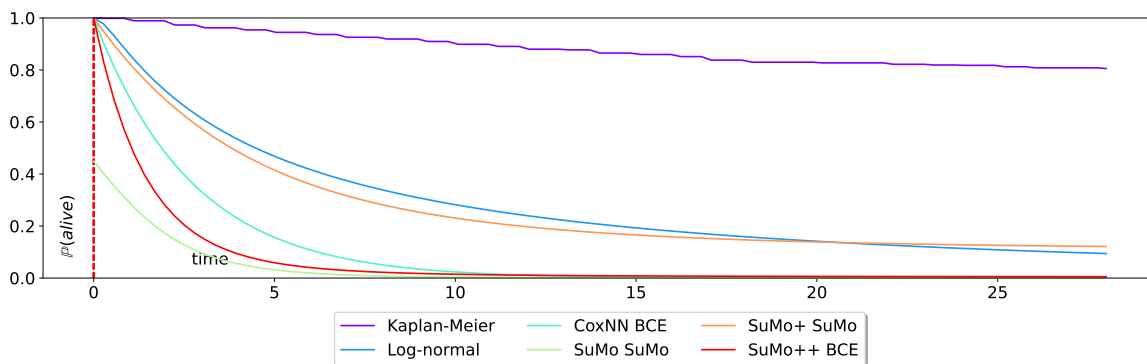


Figure 17: Survival curve examples for a sample from the COVID dataset up until T_{max} . The vertical line marks the time of the event or censoring (red: death, blue: censoring). The legend shows the model and, if applicable, the loss function (SuMo or BCE).

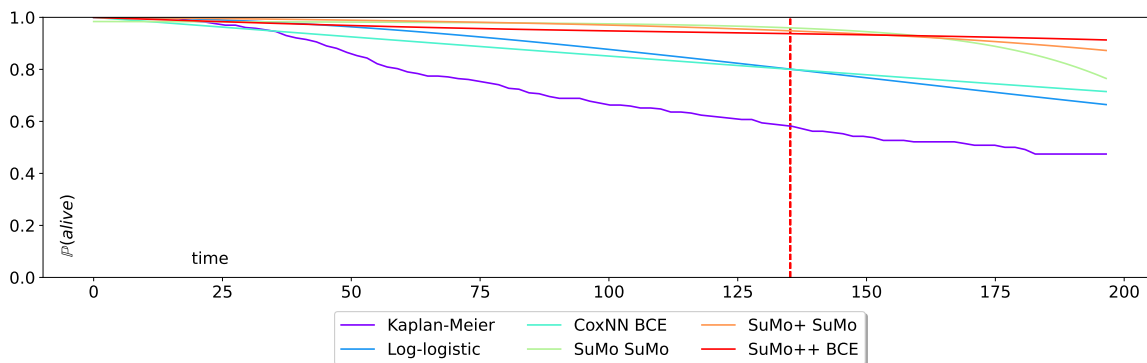


Figure 18: Survival curve examples for a sample from the GBSG2 dataset up until T_{max} . The vertical line marks the time of the event or censoring (red: death, blue: censoring). The legend shows the model and, if applicable, the loss function (SuMo or BCE).

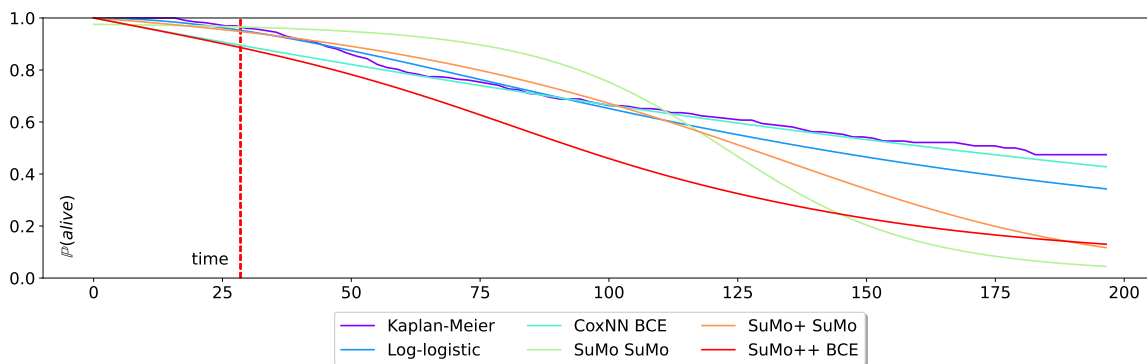


Figure 19: Survival curve examples for a sample from the GBSG2 dataset up until T_{max} . The vertical line marks the time of the event or censoring (red: death, blue: censoring). The legend shows the model and, if applicable, the loss function (SuMo or BCE).

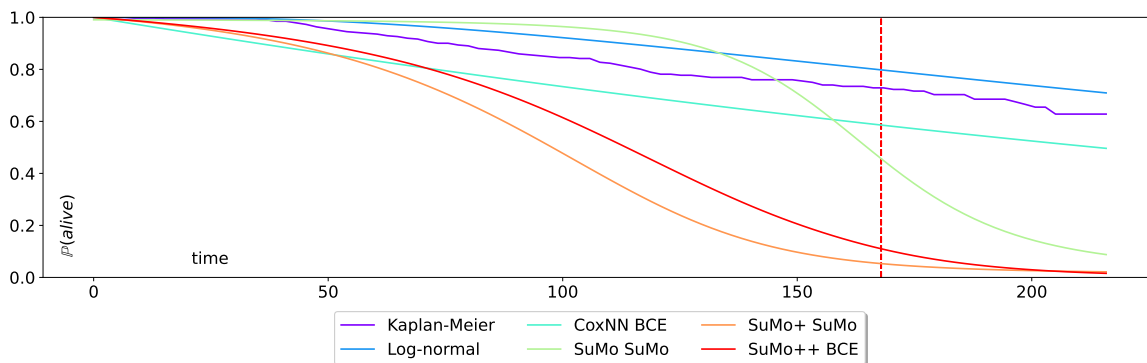


Figure 20: Survival curve examples for a sample from the Lymph dataset up until T_{max} . The vertical line marks the time of the event or censoring (red: death, blue: censoring). The legend shows the model and, if applicable, the loss function (SuMo or BCE).

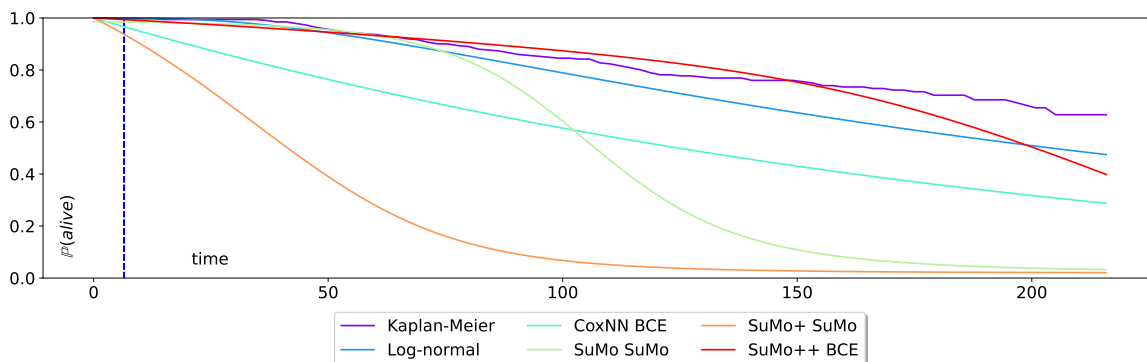


Figure 21: Survival curve examples for a sample from the Lymph dataset up until T_{max} . The vertical line marks the time of the event or censoring (red: death, blue: censoring). The legend shows the model and, if applicable, the loss function (SuMo or BCE).

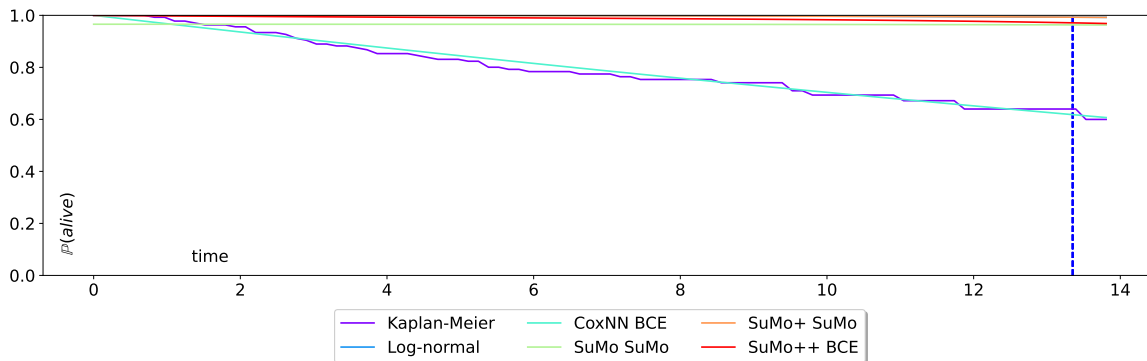


Figure 22: Survival curve examples for a sample from the NKI dataset up until T_{max} . The vertical line marks the time of the event or censoring (red: death, blue: censoring). The legend shows the model and, if applicable, the loss function (SuMo or BCE).

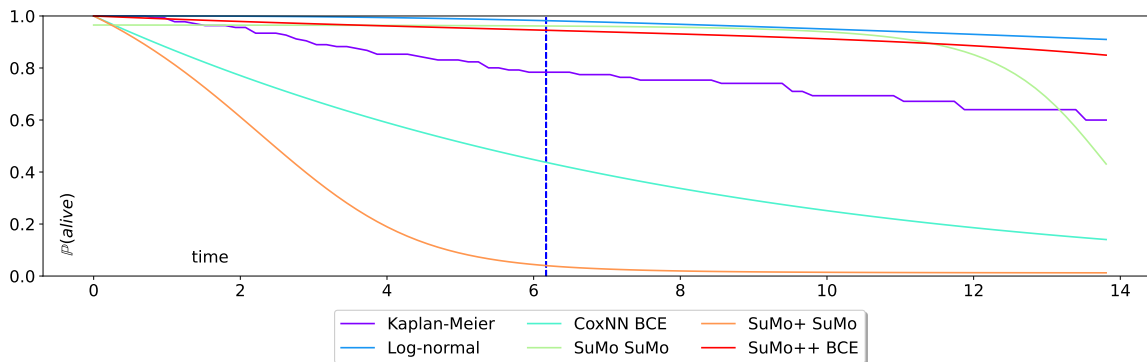


Figure 23: Survival curve examples for a sample from the NKI dataset up until T_{max} . The vertical line marks the time of the event or censoring (red: death, blue: censoring). The legend shows the model and, if applicable, the loss function (SuMo or BCE).

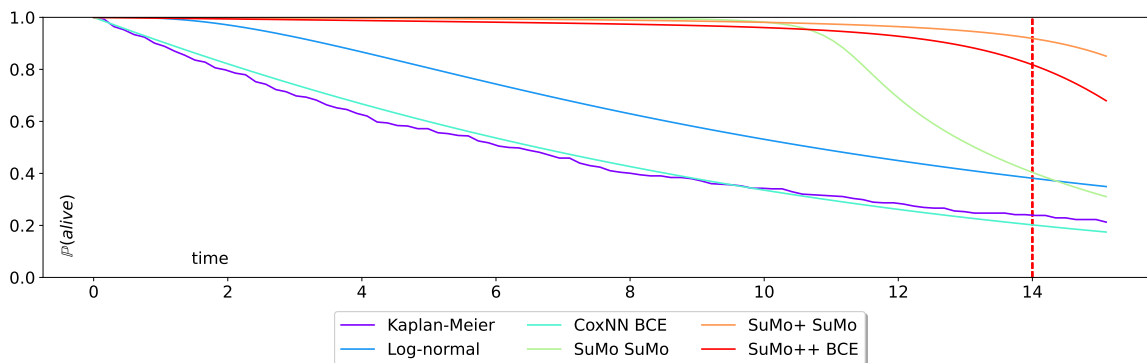


Figure 24: Survival curve examples for a sample from the Recur dataset up until T_{max} . The vertical line marks the time of the event or censoring (red: death, blue: censoring). The legend shows the model and, if applicable, the loss function (SuMo or BCE).

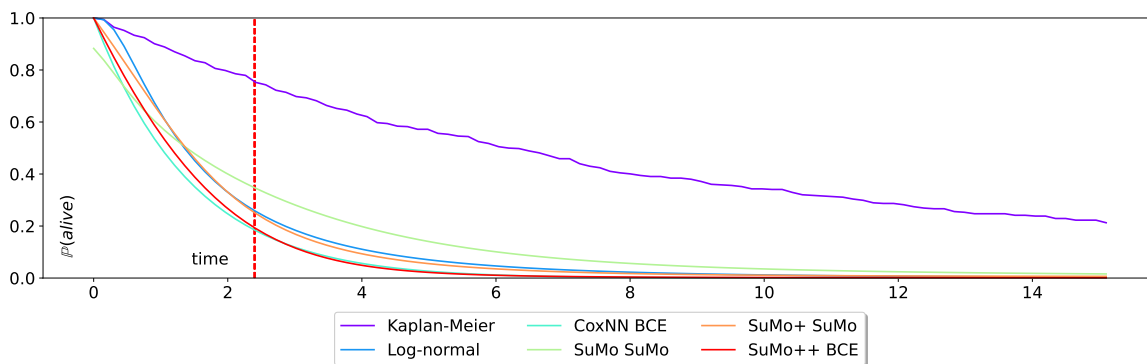


Figure 25: Survival curve examples for a sample from the Recur dataset up until T_{max} . The vertical line marks the time of the event or censoring (red: death, blue: censoring). The legend shows the model and, if applicable, the loss function (SuMo or BCE).